Working Papers

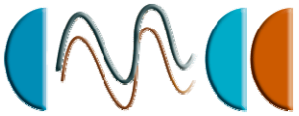

CENTRO EURO-MEDITERRANEO
PER I CAMBIAMENTI CLIMATICI

ANS – Numerical Applications and Scenarios Division

Changes in Tropical Cyclone Activity due to Global Warming: Results from a High-Resolution Coupled General Circulation Model

Silvio Gualdi

Istituto Nazionale di Geofisica e Vulcanologia ((INGV) and Numerical Applications and Scenarios Division, CMCC

Enrico Scoccimarro

Istituto Nazionale di Geofisica e Vulcanologia ((INGV) and Numerical Applications and Scenarios Division, CMCC

Antonio Navarra

Istituto Nazionale di Geofisica e Vulcanologia ((INGV) and Numerical Applications and Scenarios Division, CMCC

Centro Euro-Mediterraneo
per i Cambiamenti Climatici
www.cmcc.it

March 2007 ■ WP 8

Changes in Tropical Cyclone Activity due to Global Warming: Results from a High-Resolution Coupled General Circulation Model

Summary
This study investigates the possible changes that the greenhouse global warming might generate in the characteristics of the tropical cyclones (TCs). To this aim, scenario climate simulations, performed with a fully coupled high-resolution global general circulation model, have been analyzed. First of all the capability of the model to reproduce a reasonably realistic TC climatology has been assessed by comparing the model results from a simulation of the 20th Century with observational data sets. Then, the changes in the model TCs induced by atmospheric CO2 increase have been quantified. From the current climate simulation, the model appears to be able to simulate tropical cyclon-like vortices with many features similar to the observed TCs. The simulated TC activity exhibits realistic geographical distribution, seasonal modulation and interannual variability, suggesting that the model is able to reproduce the major basic mechanisms that link the TC occurrence with the large scale circulation. The results from the climate scenarios reveal a substantial general reduction of the TC activity when the atmospheric CO2 concentration is doubled and quadrupled. The reduction appears particularly evident for the tropical north west Pacific (NWP) and north Atlantic (ATL). In the NWP the weaker TC activity seems to be associated with a reduced efficiency of triggering of convective instabilities due to a rise of the level of free convection. In the ATL region the weaker TC activity seems to be due to both the increased stability of the atmosphere and a stronger vertical wind shear. Despite the generally reduced TC activity, there are evidences of increased intensity of the simulated cyclones in terms of rainfall. Despite the overall warming of the tropical upper ocean and the expansion of warm SSTs to the subtropics and mid-latitudes, the action of the TCS remains well confined to the tropical region and the peak of TC number remains equatorward of 20o latitude in both the Hemispheres.

Keywords: Tropical Cyclones, Global Warming, Coupled General Circulation Model.

JEL Classification:

Address for correspondence:
Silvio Gualdi
Centro Euro-Mediterraneo per i Cambiamenti Climatici
Istituto Nazionale di Geofisica e Vulcanologia
Via D. Creti, 12
40128 Bologna, Italy.
E-mail: gualdi@bo.ingv.it

Index

1. Introduction

Tropical cyclones (TCs) are non-frontal synoptic scale low-pressure systems, which develop over warm pools of the tropical or sub-tropical oceans, with organized convection and definite cyclonic surface wind circulation (Holland 1993). A severe tropical cyclone is also known as ”hurricane” in north Atlantic and north-east Pacific and ”typhoon” in west Pacific. TCs are one of the most devastating natural phenomena, which not rarely cause severe human and economic losses. Therefore, the understanding of the mechanisms that underlie their characteristics is a high-priority issue from both the scientific, social and economic point of view.

The increased frequency and intensity of observed hurricanes since 1995 (Goldenberg et al. 2001, Webster et al. 2005) and the extraordinary nature of the North Atlantic hurricane season occurred in 2005 have triggered a lively discussion about the possible changes of TC characteristics due to global climate change (e.g., Emanuel 2005, Trenberth 2005, Pielke et al. 2005, Anthes et al. 2005, Pielke et al. 2006., Landsea et al. 2006, among the others).

A number of studies have shown that TC activity varies substantially from interannual to decadal timescales. For example, sensitivity of the TC activity to El Nĩno/Southern Oscillation (ENSO) phase has been documented in several works (e.g., Gray 1984, Chan 2000, Chia and Ropelewski 2002). Similarly, low-frequency modulations of the North Atlantic Oscillation (NAO) exert significant influences on the behaviour of TCs (e.g., Elsner and Kocher 2000).

The wide interannual and decadal changes, associated with natural modes of climate variability, make difficult the identification of changes in the TC features that could be unambiguously attributed to the global warming (Walsh 2004). The detection of possible trends becomes even harder when observational data-sets only are used. The destructive nature of TCs, in fact, makes the collection of observed data extremely difficult and expansive. For this reason, databases of observed TCs are available only for a few regions (particularly North Atlantic) and are generally limited in length. Furthermore, due to subjective measurements and variable procedures, reservations have been raised about the reliability of the existing tropical cyclone data-bases for estimating climatological trends (Landesea et al. 2006).

To overcome the limitations of the observational data-sets, the possible influences of global warming on TC activity have been explored using also numerical models. Since the early work of Broccoli and Manabe (1990), a number of studies have been performed both with global and regional models, reaching controversial conclusions. Haarsma et al. (1993), for instance, found a significant increment of the number of simulated TCs in greenhouse warming experiments.

However, similar simulations, but performed with higher resolution models, showed a significant reduction of the global TC activity in a warmer earth (Bengtsson et al. 1996, Sugi et al. 2002, McDonald et al. 2005, Yoshimura et al. 2006). Royer (1998), on the other hand, found increased (decreased) TC activity in the Northern (Southern) Hemisphere, whereas Chauvin et al. (2006) showed that possible changes in the frequency of TC occurrence in the North Atlantic strongly depend on the characteristics of the sea-surface temperature (SST) spatial distribution produced by the scenario simulations.

While the issue of the TC frequency response to greenhouse warming remains arguable, some consensus has been achieved about the effects on the TC intensity. Consistent with the theoretical findings of Emanuel (1987) and Holland (1997), numerous model studies, have found that the intensity of simulated TCs tends to increase in a warmer earth (e.g., Walsh and Ryan 2000, Sugi et al. 2002, Knutson and Tuleya 2004, Chauvin et al. 2006,

Yoshimura et al. 2006, Oouchi et al. 2006). In particular, these works have shown that both the strength of the winds and the intensity of the precipitation associated with the TCs may reinforce in a warmer climate. These results appear to be rather robust, as they have been obtained using a variety of models (global and regional), different resolutions and convective parametrizations. However, it is important to note that all of these studies have been conducted analyzing experiments performed with atmospheric only models forced with prescribed SSTs, thus these experiments do not include air-sea interactions. Moreover, the SST patterns used to force the atmosphere were based on (generally low-resolution) climate scenario simulations performed with other models. This procedure, therefore, might be affected by possible inconsistencies between the simulations from which the SST patterns were taken and the atmospheric runs used to analyze the TC behaviour.

Though the air-sea feedbacks are known to be important for TC intensity (Emanuel 2003), there are only few analysis of the TC response to global warming performed with coupled models, which, moreover, have been carried out using limited area models with simplified experimental setting (Knutson et al. 2001). On the other hand, in-depth investigations of TCs and their simulation conducted with fully coupled global models, the same as those used to perform the climate scenarios, would provide further insight into these phenomena and into our ability to reproduce and predict their behaviour.

In this study, we document the ability of a high-resolution coupled atmosphere-ocean general circulation model to simulate tropical cyclone-like vortices and explore how the features of these phenomena are possibly altered by greenhouse warming. The analysis is performed on idealized greenhouse gas forcing scenarios and a simulation of the 20th Century climate. The difference with respect to the previous works published on the same subject is that we use a fully coupled model, where air-sea feedbacks are accounted for. In Section 2, a description of the model, scenario simulations and of the methodological approach used in the present paper is provided. In Section 3, we examine the ability of the model to simulate TCs. Section 4 presents an assessment of the possible changes of the TC characteristics as a consequence of global warming. In Section 5, the main findings of this work will be discussed, and the summary in Section 6 close the paper.

2. Model, Simulations and Methodology

2.1 The model

The modeling data employed in this work are time series obtained from climate simulations carried out with the SINTEX-G (SXG) coupled atmosphere-ocean general circulation model (AOGCM), which is an evolution of the SINTEX and SINTEX-F models (Gualdi et al., 2003a, 2003b; Guilyardi et al., 2003, Luo et al. 2004, Masson et al. 2005, Behera et al. 2005). The ocean model component is the reference version 8.2 of the Ocean Parallelise (OPA; Madec et al. 1998) with the ORCA2 configuration. To avoid the singularity at the North Pole, it has been transferred to two poles located on Asia and North America. The model longitude-latitude resolution is 2^{o}x2^{o} cosine(latitude) with increased meridional resolutions to 0.5^{o} near the equator. The model has 31 vertical levels ten of which lie in the top 100 m. Model physics includes a free-surface configuration (Roullet and Madec 2000) and the Gent and McWilliams (1990) scheme for isopycnal mixing. Horizontal eddy viscosity coefficient in open oceans varies from 40000 m^2s^{-1} in high latitudes to 2000 m^2s^{-1} in the equator. Vertical eddy diffusivity and viscosity coefficients are calculated from a 1.5-order turbulent closure scheme (Blanke and Delecluse 1993). For more details about the ocean model and its performance, readers are referred to Madec et al. (1998) or online to the web-site http://www.lodyc.jussieu.fr/opa/.

The evolution of the sea-ice is described by the LIM (Louvain-La-Neuve sea-ice model; Fichefet and Morales Maqueda, 1999), which is a thermodynamic-dynamic snow sea-ice model, with three vertical levels (one snow and two ices). The model allows for the presence of leads within the ice pack. Vertical and lateral growth and decay rates of the ice are obtained from prognostic energy budgets at both the bottom and surface boundaries of the snow-ice cover and in leads. When the snow load is sufficiently large to depress the snow-ice interface under the sea-water level, sea-water is supposed to infiltrate the entirety of the submerged snow and to freeze there, forming a snow ice cap. For the momentum balance, sea-ice is considered as a two-dimensional continuum in dynamical interaction with atmosphere and ocean. The ice momentum equation is solved on the same horizontal grid as the ocean model. LIM has been thoroughly validated for both Arctic and Antarctic conditions, and has been used in a number of process studies and coupled simulations (Timmermann et al. 2005 and references therein).

The atmospheric model component is the latest version of ECHAM-4 in which the Message Passing Interface (MPI) is applied to parallel computation (Roeckner et al. 1996). We adopted a horizontal resolution T106, corresponding to a gaussian of about 1.12^{o}x1.12^{o}. In the contest of long coupled climate simulations, this is a considerably high horizontal resolution. A hybrid sigma-pressure vertical coordinate is used with 4-5 of a total of 19 levels lying in the planetary boundary layer. The parameterization of convection is based on the mass flux concept (Tiedtke, 1989), modified following Nordeng (1994). The Morcrette (1991) radiation scheme is used with the insertion of greenhouse gases (ghg) and a revised parameterization for the water vapour and the optical properties of clouds. A detailed discussion of the model physics and performances can be found in Roeckner et al. (1996).

The vertical turbulent transfer of momentum, mass, water vapour and cloud water is based on the similarity theory of Monin-Obhukov (Louis, 1979). The effect of the orographically induced gravity waves on momentum is parameterized by a linear theory and dimensional considerations (Miller et al., 1989). The soil model parameterizes the content of heat and water in the soil, the continental snow depth and the heat of permanent ice over continents and seas (Dumenil and Todini, 1992). The vegetation effects are parameterized following Blondin (1989).

The ocean and atmosphere components exchange SST, surface momentum, heat and water fluxes every 2 hours. The coupling and the interpolation of the coupling fields is made through the OASIS2.4 coupler (Valcke et al., 2000). No flux corrections are applied to the coupled model.

2.2 The climate scenario simulations

With respect to the previous versions of the SINTEX model, SXG includes a model of the sea–ice, which allows the production of fully coupled climate scenario experiments. In this paper, we present results obtained from the analysis of four climate simulations (Table 1).

In order to assess the capability of the model to reproduce a reasonably realistic TC activity and to evaluate the effectiveness of our TC detection methodology, the tropical cyclone-like vortices produced during the last 30 years of a 20th Century simulation have been analyzed and compared with observations. The simulation has been conducted integrating the model with forcing agents, which include greenhouse gases (CO_2 , CH4 , N2O and CFCs) and sulfate aerosols, as specified in the protocol for the 20C3M experiment defined for the IPCC simulations (for more details see also the website http://www-pcmdi.llnl.gov/ipcc/about ipcc.php). The integration starts from an equilibrium

state obtained from a long coupled simulation of the pre-industrial climate, and has been conducted throughout the period 1860-2000.

Once the skill of the model to reproduce TC-like vortices has been evaluated using the present climate simulation, the possible effects induced by greenhouse global warming on the simulated TCs have been explored using 30 years of twice-daily data from climate scenario experiments. Specifically, a simulation with atmospheric CO_2 concentration 287 ppm, corresponding to the pre-industrial period (PREIND), a climate simulation with CO_2 concentration doubled with respect to the PREIND period (2CO2), and a climate simulation with atmospheric CO_2 concentration quadrupled with respect to the PREIND period (4CO2). The transition between PREIND and 2CO2 and between 2CO2 and 4CO2 periods has been produced by a 1%/year increment of the CO_2 concentration. At the end of the two transition periods, the model has been integrated for 100 years with constant values of CO_2 concentration, i.e. 574 ppm and 1148 ppm respectively.

A greenhouse warming scenario based on a doubling and a quadrupling of atmospheric CO_2 is certainly an idealized experiment and does not represent a realistic forecast of future radiative forcing. The motivation of this choice resides in the fact that large concentration of atmospheric CO_2 might emphasize and make more evident the response of simulated TCs to greenhouse warming. Also, the advisability of this kind of idealized experiments in the framework of TC studies has been discussed by Michaels et al. (2005) and Knutson and Tuleya (2005). Furthermore, the possible impacts of a doubling of atmospheric CO_2 concentration has been explored in a number of previous works (e.g., Broccoli and Manabe 1990, Haarsma et al. 1993, Bengtsson et al. 1996, Royer 1998, Sugi et al. 2002, Knutson and Tuleya 2004, McDonald et al. 2005, Yoshimura et al. 2006, Chauvin et al. 2006), but so far no analysis has been performed on the effects of its further increase.

Figure 1 shows the time series of the annual mean values of surface temperature averaged over all latitudes and longitudes, from year 1870 to year 2000, for the model simulation and observations (Jones et al. 2001). The curves represent the year-to-year deviation of the annual mean with respect to the 1870-1890 mean. The observations (dashed curve) show the well known global warming trend of about 0.6 ^{o}C over the past century. The model simulation (solid curve) exhibits a similar trend, though slightly more pronounced, over the same period. Analogous results are found for the sea-surface temperature (SST) field (not shown).

2.3 Reference data

The simulated TC-like vortices and the main features of their climatology are evaluated comparing the model results with observational data sets. Specifically, we use a global TC data set obtained from the Unisys Corporation website (http://weather.unisys.com/hurricane/).

This data set has been produced collecting observational data from the National Hurricane Center (NHC), the U.S. National Oceanic and Atmospheric Administration (NOAA) and the U.S. Joint Typhoon Warning Center (JTWC), and has already been used in a similar analysis study by Oouchi et al. (2006). In the rest of the paper the results obtained from this data set will be referred to as ”observations”.

Furthermore, the capability of the model to reproduce the observed mean climate is assessed using the ECMWF 40-year Re-Analysis (ERA40; more information available at the website http://www.ecmwf.int/research/era), the observational sea-surface temperature data set HadISST (Global Sea-Ice and Sea Surface Temperature Dataset produced at the Hadely Centre, Rayner et al. 2003) and the observed precipitation data set produce by Xie

and Arkin (1997). For the sake of simplicity, in the rest of the paper we will refer to all of these data as observations.

2.4 Method of detection of the simulated Tropical Cyclones

Basically, two methods for detecting TCs have been commonly used in the analysis of general circulation model (GCM) experiment results. The first technique produces an estimate of the TC activity based on a genesis parameter computed from seasonal means of large scale fields (Gray 1979, Watterson et al. 1995, Royer 1998). This method has been used especially in the analysis of low-resolution model runs, as it obviates the explicit simulation of individual TCs. The second method is the location and tracking of individual TCs based on objective criteria for the identification of specific atmospheric conditions that characterize a TC with respect to other atmospheric disturbances. In particular, TCs are identified and tracked as centres of maximum relative vorticities and minimum of surface pressure, with a warm core in high levels and maximum wind in the low layers of the atmosphere (Haarsma 1993, Bengtsson et al. 1995, Walsh 1997). In the existing literature, the definition of the criteria, i.e. the thresholds and the domain over which they are computed, varies from work to work. A discussion and a short summary for the criteria of objective TCs detection in atmospheric analysis and model simulations is given in Walsh (1997) and Chauvin et al. (2006) respectively. In this study, we use a TC location and tracking method based on the approach defined in Bengtsson et al. (1995) and Walsh (1997). Specifically we assume that a model TC is active over a certain grid point A if the following conditions are satisfied:

1. In A relative vorticity at 850 hPa is $> 3 \cdot 10^{-5}$ s^{-1} ;
2. There is a relative minimum of surface pressure and wind velocity is > 14 m/s in an area of 2.25° around A;
3. Wind velocity at 850 hPa is > wind velocity at 300 hPa ;
4. The sum of temperature anomalies at 700, 500 and 300 hPa is > 2 °K. Where the anomalies are defined as the deviation from a spatial mean computed over an area of 13 grid points in the east-west and 2 grid points in the north-south direction;
5. Temperature anomaly at 300 hPa is > temperature anomaly at 850 hPa ;
6. The above conditions persist for a period longer than 1.5 days ;

The choice of the parameters in conditions 1-6 are very similar to the value indicated by Bengtsson et al. (1995) and Walsh (1997) and optimize the detection of simulated TCs in our model compared with the observations. Also, we checked the sensitivity of our results to small changes in these parameters. We found that the number of detected TCs is scarcely sensitive to the threshold values, but exhibits some sensitivity to the size of the areas over which means are computed. For a complete discussion of these criteria and their sensitivity to the parameters used the reader is addressed to Walsh (1997).

3. Simulation of the tropical climate and TC climatology

As a first step we assess and discuss the capability of the model to reproduce the main features of the observed tropical climate and TC climatology. To this aim, we analyze the results obtained from a simulation of the 20th Century, as described in Section 2.2, comparing the model results with observations (re-analysis) for the period 1970-1999.

The TC occurrence has a pronounced seasonal character, with more intense activity found in the summer hemisphere (Emanuel 2003), namely in the Northern Hemisphere

from June to October and in the Southern Hemisphere from December to April. Therefore, we will focus our attention on the specific seasons (and regions) of intense TC activity.

3.1 Simulation of mean state and high-frequency variability in the Tropics

Figure 2 shows the seasonal means of SST and precipitation as obtained from the observations and the model, for the extended northern summer (June-October, JJASO) and southern summer (December-April, DJFMA).

In general the model overestimates the SSTs in the tropical regions, during both seasons.

The seasonal mean SST, averaged over the tropics is 0.26^{o}C and 0.32^{o}C warmer than observed in JJASO and in DJFMA respectively. The warm bias is visible both in the tropical Indian Ocean and Atlantic Ocean, but it becomes particularly evident in the central-eastern Pacific, south of the equator. In this region over, the warm SSTs, the model overestimates also the rainfall, tending to produce a double ITCZ, which is a common error of most AOGCMs. In the equatorial Pacific, on the other hand, the model cold tongue is clearly too strong and extends too far west. Correspondingly, the simulated precipitation is too weak in the equatorial Pacific, especially west of the date line.

In the tropical Atlantic, the model rainfall is reasonably close to observations in JJASO, whereas during DJFMA it appears to be shifted south (by about 10^{o} of latitude), probably as a consequence of the excessively warm SSTs found in the subtropical southern Atlantic, off the Brazilian coast. Interestingly, in the tropical Indian Ocean, the model precipitation is generally weaker than observed. During northern summer, the model shows a clear rainfall deficit in the area affected by the Asian summer monsoon, extending from the Bay of Bengal, through South-east Asia and South China Sea, up to the region east of the Philippines archipelago.

Simulated precipitation appears to be too weak also over the eastern equatorial Indian Ocean, whereas it tends to be too intense in the western part of the basin, between the equator and 10^{o} S. Also during northern winter (Figure 2, panels g and h) model rainfall is too weak over the eastern Indian Ocean and the Indonesian region.

A first estimate of the variability of the convective activity can be obtained from the standard deviation of the out-going longwave radiation (OLR). Figure 3 shows the standard deviation of OLR, for observations (left column) and model simulation (right column), as obtained from daily anomalies. In the observation, the pattern of total variability (panel a) shows maxima over the eastern Indian ocean, from the equatorial region to the Bay of Bengal and over the western Pacific, extending from the Philippines south-eastward along the Southern Pacific Convergence Zone (SPCZ) and eastward along the ITCZ. Secondary maxima are found over tropical West Africa (the region of the African monsoon), and in the extra-tropics over South and North America, along the western Atlantic coast. The model (panel b), exhibits some tendency to overestimate the OLR variability. However, the location of the model maxima is mostly consistent with the observations. In the Tropics, the excess of simulated convective variability is particularly noticeable in the central Pacific, south of the equator and east of the date line, in the western Atlantic and western Indian Ocean. The standard deviations of the daily OLR anomalies shown in Figure 3 (upper panels) give an estimate of the convective variability at all time scales. In this work, however, we are specifically interested in phenomena that have relatively short time scales, on the order of (few) weeks. Thus, in order to highlight the high-frequency convective variability, the OLR anomalies have been high-pass filtered before computing the standard deviations. The patterns of the high-frequency variability are shown in Figure 3, middle and lower panels for the northern summer and southern

summer respectively, both for the model and observations. Also in this case, the model exhibits some ability in capturing the distribution of convective variability.

In particular, during northern summer the the simulated high-frequency convective variability appears to be quite realistic, with maxima located in the western tropical Pacific, along the

Pacific and Atlantic ITCZ and along the storm tracks in the winter hemisphere. During southern summer the model tends to overestimate the variability, especially in the subtropical central Pacific and in the mid-latitude northern Pacific.

3.2 Simulation of Tropical Cyclones

In this Section we analyze the ability of the model to simulate tropical cyclones-like vortices (that we will refer to simply as TCs), following the methodology discussed in Section 2.4. As a first step, we compare the total number of TCs per year detected in the model simulation and in the observations over the period 1970-1999 (Table 2). In general, the number of simulated TCs per year is almost 30% lower than the number detected in the observations, whereas the interannual variability of TC number is quite well captured by the model. The lower number of simulated TCs is consistent with the results found in other model studies, where atmospheric only models were used (e.g., Bengtsson et al. 1996, Camargo et al. 2004), though in our case the difference between observed and simulated number is considerably smaller. The geographical distribution of the TCs formation positions is shown in Figure 4. In the observations (panel a) there are four distinct regions of TCs formation in the Tropics of the Northern Hemisphere: North Indian Ocean (NI), West-North Pacific (WNP), East- North Pacific (ENP) and North Atlantic (Atl); and three regions in the Southern Hemisphere: Southern Indian Ocean (SI), the ocean north of Australia (AUS) and the Southern Pacific (SP).

Based on these regions of TCs genesis and following Camargo et al. (2004), we define seven basins (demarked by the boxes in Figure 4) that will be used to delimit and characterize the different areas of TCs activity.

The model (Figure 4, panel b) reproduces well the patterns of TCs genesis, especially in the Northern Hemisphere. The ma jor contrast with the results obtained from the observations occurs in the southern Atlantic, where the model generates some TC, though no TCs are observed in this region during the considered period (1970-1999). This model error might be related to the too warm SSTs and intense convective activity found in this region (Figure 2).

A comparison with the results obtained with atmospheric only model forced with observed SSTs (Camargo et al. 2004, Figure 2) shows a substantial improvement in the patterns of TC genesis obtained with the coupled simulation. Interestingly, the comparison is made more valid by the fact that one of the atmospheric models used in Camargo et al. (Echam4) is basically the same as the one we use as atmospheric component in our coupled model. An important difference, however, is the horizontal resolution, which is T42 in Camargo et al. and T106 in our case. The enhanced model resolution might explain some of the improvements we find with our model, such as, for example, the increased global number of TCs, accompanied by a significant reduction of the number of TCs near the equator, which is a rather unrealistic feature.

In Figure 5, the box plots representing the mean number of TCs per year for each activity area are shown both for the observations (left panel) and the model (right panel). The plots confirm that in the simulation there is a lower number of TCs, especially in the tropical north Pacific (WNP and ENP). However, in general the difference with the observations is relatively small, and, for each area, the model simulates a fairly realistic mean year-to-year variability (see also STD in Table 2). More importantly, the simulation

appears to capture the basic features of the TC distribution among the different areas. Specifically, the region with the highest mean number of TCs per year is the north-western tropical Pacific (WNP) both in the model and observations. Also the mean number of TCs in the north Indian Ocean (NI) and Atlantic region (ATL) are well reproduced, whereas the TC activity in the north-eastern Pacific (ENP) is cleary underestimated.

The main objective of this Section is to assess how good the model is in simulating the basic features of the mean tropical climate and of the TCs climatology. The results shown in Figures 2-5 indicate that the model reproduces a quite realistic tropical mean state (at least in terms of SST and precipitation) and number of simulated TC-like vortices. Furthermore, the geographic distribution of TCs appears to be in good agreement with the observations. However, so far nothing has been said about how realistic the features of a simulated TC are. In order to have a closer look at the structure of the model TCs, Figure 6 depicts the composite patterns of precipitation and low-level wind fields associated with a model TC.

The composites were calculated by averaging the fields over the period of occurrence of a TC and for a domain centered on the core of the cyclone and extending 10^{o} each side. The TC used for the composite computation has been chosen randomly from the simulated TCs, and a visual inspection of the composite patterns obtained from several other model TCs (for different simulation periods and regions) indicate that the results shown in Figure 6 are fairly representative of the mean simulated TC.

From the patterns in Figure 6 it turns out that the model simulates TCs with a fairly realistic structures. When averaged on its lifetime, the simulated TC has intense mean precipitation and surface winds that extend for about 300-400 Km from the centre (”eye”) of the cyclone. The amplitude of the fields is substantially smaller than observed, but consistent with the results obtained from high-resolution atmospheric GCMs experiments (e. g., Bengtsson et al. 1995, Chauvin et al. 2006). In agreement with observational studies (e.g., Frank 1977, Gray 1979, Willoughby et al. 1982), the strongest wind velocities are located to the (north-)east of the core, though the maxima in the model is much too far away from the ”eye”. This model error is most likely due to the model resolution, which does not allow to resolve the fine and tight structures observed in ”real” TCs, as also suggested in McDonald et al. (2002) and Chauvin et al. (2006). For the same reason, the simulated TC does not exhibits the ”eye” in precipitation, though in general the rainfall pattern is reasonably realistic. An important feature of the observed TCs is their marked seasonal character (Emanuel 2003). Figure 7 shows the seasonality of TC occurrence for both observations and model simulations in the Northern Hemisphere and Southern Hemisphere and for specific regions of activity described in Figure 4. In general the model reproduces well the seasonal behaviour of TCs, especially in the Southern Hemisphere, the northern Indian and Atlantic Oceans. In the Northern Hemisphere, and particularly in the north-west and north-east Pacific the annual phase of the TC activity is captured but the amplitude is much smaller, consitent with the reduced numebr of simulated TCs previously discussed. Beside the seasonal modulation, the TC activity exhibits a rather strong year-to-year variability. As it has been shown in a number of studies (Gray 1984, Chan 2000, Chia and Ropelewski 2002, among the others), this interannual variability has a strong link with ENSO.

Changes in the SST distribution in the tropical Pacific and the associated changes in the large scale circulation, in fact, appear to have a strong impact on the number of TCs that occur in different regions of the globe. The relationship between ENSO and TCs activity differs depending on the region considered. The number of observed TCs in the north Atlantic, for instance, is negatively correlated with the NINO3 ENSO index, whereas

the number of TCs in the north-east Pacific is positively correlated with the same ENSO index.

Figure 8 shows the interannual variation of the number of TCs in the north Atlantic, north-east Pacific and southern Indian Ocean (solid curves), along with the NINO3 SSTA index (dotted curves).Here, the value of the NINO3 index is computed for the season of maximum TC activity, i.e. JJASO for the Northern Hemisphere and DJFMA for the Southern Hemisphere.

The curves shown in Figure 8 indicate that the model simulates a fairly realistic interannual modulation of the number of TCs and that this interannual variability is correlated with ENSO similarly to what is found in the observations.

All these results indicate that the model simulates intense convective disturbances with characteristics similar to the basic features of observed TCs, reassuring about its suitability to investigate how climate change might impact on the TC activity, which will be the subject of the next Section.

4. Impacts of the global warming on the tropical climate and TC climatology

Possible changes in the basic features of the tropical mean climate and of the simulated tropical cyclones due to greenhouse global warming are investigated using the climate scenario experiments PREIND, 2CO2 and 4CO2 described in Section 2.2. Figure 9 shows the the time series of the annual mean values of surface temperature averaged over all latitudes and longitudes for the scenarios along with the 20C3M simulation. The curves represent the year-to-year deviation of the annual mean with respect to the 1840-1870 mean, i.e. the mean of the last 30 years of the PREIND period.

As already discussed in Section 2.2, during the 20th Century the model simulates a global warming reasonably realistic (Figure 9, dashed-dotted curve), though slightly more pronounced than observed. The $1\%/yr^{-1}$

CO_2 increment produces a much larger impact on the global temperature. In the CO_2 experiment (solid curve), after having doubled the CO_2 concentration, during the stabilization period, the global mean temperature at the earth surface is about 2 ^oC warmer than in the preindustrial simulation. A warming larger than 4 ^oC, then, is obtained when the CO_2 is quadrupled (4CO2, dotted curve).

4.1 Changes in the tropical mean state

The impacts of the increased atmospheric CO_2 on the mean state of the Tropics is shown in Figure 10. Here the difference between 2CO2 and PREIND (2CO2-PREIND), and 4CO2 and PREIND (4CO2-PREIND) seasonal means of SST and precipitation are shown. Panels a, b, e and f indicate that the overall warming of the tropical SST is characterized by regional patterns. Both during JJASO and DJFMA, in fact, the warming is more marked in the western part of the Indian Ocean, in the equatorial Pacific and along the coast of South America, whereas a weaker warming is found in the eastern tropical Indian Ocean and eastern subtropical Pacific.

In the tropical Pacific the warming patterns resemble El Nino anomalies. Interestingly, these patterns are similar for the 2CO2-PREIND and 4CO2-PREIND cases, though with different amplitudes.

Similar characteristics exhibit the patterns of difference between the PREIND, 2CO2 and 4CO2 precipitation (panels c, d, g and h). In particular, the increased CO_2 induces a remarkable enhancement of precipitation along the ITCZ, from the Indian Ocean, through the Pacific to the Atlantic, during JJASO. Interestingly the increase of rainfall is confined to a relatively narrow region, very close to the equator. In the same season, areas of reduced rainfall are located in the south-eastern tropical Indian Ocean and south-central Pacific.

During DJFMA, increased precipitation is found south of the equator, along the southern branch of the double ITCZ simulated by the model and discussed in Section 3.1; whereas regions of decreased rainfall are found in the subtropics of both the summer and winter hemispheres. Also in this case, the patterns of precipitation difference 2CO2-PREIND and 4CO2-PREIND exhibit very similar spatial features but different amplitudes.

Table 3 shows the changes in mean temperature, mean precipitation and mean convective precipitation over the entire globe and over the Tropics for the three experiments. Interestingly, while a substantial rise in mean surface temperature and mean total precipitation are found when the CO_2 is increased, a completely different behaviour is found for the convective precipitation. The latter in fact shows a significant reduction when the atmospheric CO_2 concentration has doubled and quadrupled, especially in the tropical region.

Figure 11 shows the changes in high-frequency convective variability induced by the CO_2 forcing in terms of difference in standard deviation of high-pass filtered OLR anomalies. For the sake of brevity, only the difference between 4CO2 and PREIND period is considered (2CO2-PREIND produces very similar patterns, but smaller amplitude). Over most of the tropical belt the sign of the difference is negative, indicating a tendency of the model to attenuate the high-frequency convective variability when the atmospheric CO_2 has increased. Only over the equatorial Pacific, between about 5 ^{o}N and 5^{o}S, there is a clear sign of enhanced variability.

These results appear to suggest that increasing the concentration of CO_2 in the atmosphere of the model, the general warming of the earth surface is accompanied by a reduction of the (deep) convective activity in the Tropics. The weaker convective activity, in turn, might be due to an enhancement of the vertical stability of the atmosphere. This point will be discussed more in detail in Section 5.

4.2 Changes in the simulated tropical cyclones

Let us consider now what happens to the simulated TCs as a consequence of the greenhouse global warming. Table 4 shows the total number of TCs and TC days (upper row), the annual mean number of TCs and TC days (middle row) and their standard deviations (lower row) for the PREIND, 2CO2 and 4CO2 experiments. Both the total number and the annual mean number of TCs and TC days appear to be substantially reduced with increased concentration of atmospheric CO_2 , whereas their interannual variability does not show significant changes. Our simulations, thus, indicate that increased CO_2 leads to a reduction of the TC activity, both in terms of number of TCs and number of TC days. These results are consistent with previous findings (e.g., Bengtsson et al. 1996, Sugi et al. 2002, McDonald et al. 2005, Yoshimura et al. 2006), and for the first time they have been obtained using climate scenario simulations performed with a state-of-the-art fully coupled GCM.

The box plots shown in Figure 12 represent the mean number of TCs per year for each activity area and for the three climate experiments. The reduction of the number of TCs is visible in all of the regions, though it appears to be particularly evident in the WNP and ATL areas.

Generally, it is accepted that TCs tend to develop over oceanic warm waters (e.g., Palmen 1948). Specifically, climatological studies indicate that the SST has to be warmer than about 26 ^{o}C. The overall warming of the SST shown in Figure 10, implies a poleward migration of the 26 ^{o}C isotherm, therefore, one could expect to find a polward extension of the TC activity in a warmer climate.

Figure 13 shows the zonal average of the total number of simulated TCs (dashed lines) along with the zonal mean SST (solid lines) for the three experiments, PREIND

(upper panel), 2CO2 (middle panel) and 4CO2 (lower panel). In the PREIND case the zonal mean SST threshold for TC occurrence appears to be between 25 and 26 ^{o}C. The maximum number of TCs occurs slightly equatorward of 20^{o} latitude in both Hemispheres.

Increasing the atmospheric CO_2 (middle and lower panels) the 26 ^{o}C isotherm migrates poleward, on average, of almost 10^{o} of latitude, but the latitudinal distribution of the TC number does not appear to be substantially changed. The maxima of TC occurrence, though substantially reduced, still appears to be confined equatorward of 20^{o} latitude. On the other hand, the zonal mean SST threshold for TC occurrence increases to about 28 ^{o}C and almost 30 ^{o}C for the 2CO2 and 4CO2 cases respectively. These results suggest that the poleward migration of warm SSTs caused by the greenhouse global warming does not imply an extension of the regions of cyclogenesys towards the middle latitudes. Similar findings for the relationship
between SSTs and convective precipitation have been shown in Dutton et al. (2000).
In order to assess possible modifications in the strength of the simulated TCs, we have analyzed the changes in intensity of both low-level winds and convective precipitation associated with the model TCs. The intensity of the TC low-level wind has been analyzed using the PDI (power dissipation index) proposed by Emanuel (2005), whereas as an index of intensity of TC precipitation we consider the convective rainfall averaged over a 4 by 4 grid point area around the centre of the cyclone and over the duration of the event.

When the pdf (probability distribution function) of the PDI for the three experiments are computed and plotted (not shown), the curves do not show substantial differences. In other words, in terms of strength of the near-surface wind, the changes in atmospheric CO_2 do not appear to alterate the intensity of the simulated TCs. A different result is obtained when we use the convective precipitation to quantify the intensity of the model TCs.

Figure 14 shows the pdf of convective precipitation associated with a model TC for four different regions of activity and for the three experiments. In all of the cases, the maximum of pdf appears to shift to higher values of convective rainfall when the CO_2 increases. To further confirm these findings, in Figure 15 the composite of TC precipitation are shown.

Specifically, the shaded patterns show the composites of TC rainfall for the PREIND case, whereas the contours are the difference between the composite 2CO2-PREIND (upper panels) and 4CO2-PREIND (lower panels), for the WNP region (left panels and the ATL region (right panels). Using a boot-strap technique, the changes shown in Figure 14 are found to be sta- tistically significant, and suggest that the amount of TC rainfall, on average, becames larger as a consequence of the greenhouse warming. Thse results are consistent with the findings of Chauvin et al. (2006), for the Atlantic hurricanes, and Yoshimura et al. (2006), who used a high-resolution atmospheric only model.

5. Discussion

In Section 4, it has been shown that, in general, the frequency of the simulated TCs is substantially and significantly reduced when the concentration of atmospheric CO2 is increased. In order to understand this result, in this section we analyze and discuss how the global warming affects those characteristics of the tropical atmosphere which are of relevance for the development of the TCs. In particular, here we consider the two ma jor basic mechanisms, dynamical and thermodynamical, that can oppose the development, and hence the occurrence, of these phenomena: the vertical wind shear and the stability of the atmosphere.

It is well known that the vertical wind shear is one of the dynamical parameters that controls the formation of TCs. Specifically, strong large scale vertical wind shear represent

unfavorable environmental conditions to the development of TCs (Gray 1968, Emanuel 2003). Therefore, a change in the climatological wind shear induced by greenhouse warming over a certain region might affect the TC frequency there.

Figure 16 shows the vertical wind shear for the PREIND and 4CO2 experiments and the difference 4CO2-PREIND (for the sake of brevity, here we omit the 2CO2 experiment, whose results are fully consistent with the 4CO2 case, though with smaller amplitudes). Both in the PREIND and 4CO2 case, the Tropics are characterized by a minimum of vertical wind shear, which is particularly weak in the summer hemisphere. The difference 4CO2-PREIND (bottom panels) indicates a general reduction of the wind shear over most of the Tropics. This result is in agreement with previous studies, which have shown the weakening of the tropical circulation with the increasing of the atmospheric CO2 (e. g. Knutson and Manabe 1995, Vecchi and Soden 2007).

A notable exception is the reinforcement of the vertical wind shear in the 4CO2 experiment visible both in winter and in summer over the north tropical Atlantic. Thus, the stronger wind shear might be one of the possible causes of the TCs reduction found over this area.

Interestingly, the warming patterns in the tropical Pacific SSTs found in the 4CO2 case (Figure 10) resemble the SST anomalies occurring during El Nino events. It is known that ENSO affects the TC activity over the north tropical Atlantic and one hypothesized mechanism is the modulation of the vertical wind shear strength (Goldenberg and Shapiro 1996). Therefore, the stronger response of the tropical eastern Pacific SSTs to the global warming might induce a reduction of the TC activity in the ATL region in a way (and through mechanisms) similar to the influence exerted by El Nino (see also Aiyyer and Thorncroft 2006, Latif et al. 2007). The strengthen of the vertical wind shear, however, does not explain the reduction of the TCs over the WNP. Figure 16, in fact, shows that the wind shear reinforces over this region only during the northern winter, whereas it remains substantially unalterated in boreal summer, i.e. the TC season for this area. Therefore, there must be some other explanation for the reduced TC activity in this area. Another important parameter that may regulate the development of TCs is the vertical stability of the atmospheric column (e.g., Gray 1979, De Maria 2001). If the atmosphere becomes more stable, the occurrence of phenomena based on the development of organized convective systems, such as TCs, becomes more unlikely. The vertical profiles of the equivalent potential temperature (θe) computed over the areas and for the season of TC activity (not shown) indicate that the atmospheric column is, on average, conditionally unstable in all of the cases (PREIND, 2CO2 and 4CO2).

However, as it shown in Figure 17, the level of free convection (LFC) over the WNP and ATL areas tends to be higher when the atmospheric CO2 concentration has been increased.

The effects of the higher LFCs that characterize these regions, and particularly the WNP, is to reduce the chance for convective instabilities to develop. This result is consistent with the general reduction of convective precipitation discussed in Section 4.1 and explains the weaker TC activity in the WNP area. For the ATL region, on the other hand, the decreased number of TCs appears to be probably due to both the increased vertical wind shear and the reduced instability of the atmosphere.

Finally, the changes in the LFC induced by the CO2 increase and the subsequent reduction of convective activity is consistent with the findings of other sutdies, where the effects of atmospheric CO2 concentration on the tropical convection have been investigated (e.g., Knutson and Manabe 1995, Sugi and Yoshimura 2004).

The increased intensity of TC precipitation, found in Section 4.2 (Figure 14 and Figure 15), is only apparently in contraddiction with the reduced convective activity of the

tropical atmosphere induced by the CO2 increase. Our results indicate that the rise of the LFC due to the CO2 increase make more difficult the trigger of convective episodes. On the other hand, the warming of the tropical troposphere is accompanied by an increase of water vapor. Therefore, when the convective process is somehow activated the larger amount of moisture available in the 2CO and 4CO2 atmosphere makes the precipitation more intense.

6. Summary

In this study, we use a fully coupled high-resolution AOGCM to investigate the possible impacts of greenhouse global warming on the characteristics of tropical cyclones. To our knowledge, this is the first time the impact of global warming on TCs is investigated by means of a state of the art fully coupled GCM.

The simulated TCs have many, basic, gross features similar to the observed ones. However, the rather low intensity of the low-level winds and the too large distance between the cyclone eye and the wind maximum remain unsatisfactory. These shortcomings are likely due to the model resolution, which, though rather high for long climate simulations, is still too coarse for an adequate representation of the tight structures accompanying these phenomena. Despite these problems, the model seems to be able to simulate a reasonable realistic climatology of TCs, both in terms of spatial distribution, seasonal and interannual variability of the TC activity.

In particular, the model appears to capture at least some of the links between SST interannual variability and TC activity.

The increased concentration of amospheric CO2 induces a warming of the entire tropical and subtropical upper ocean, accompanied by a redistribution of the tropical rainfall. The increase of the tropical ocean surface temperature, however, is not uniform, and the eastern Pacific exhibits a more prononced warming with patterns that resemble El Nino SST anomalies. The total precipitation averaged over the Tropics increases with the CO2 increase, but the convective precipitation exhibits a significant reduction.

Along with the attenuated convective activity, our simulations show a substantial and significant reduction of the number of generated TCs, especially over the North West Pacific and North Atlantic tropical regions. The weaker TC activity in the NWP area appears to be related to an increased convective stability, whereas the reduced TCs in the ATL might be associated to both increased stability of the atmospheric column and increased vertical wind shear over this region. The increased vertical wind shear over the tropical north Atlantic is consistent with the change in the SST distribution induced by the greenhous global warming and specifically with the El Nino like pattern of warmer SST found over the tropical esatern Pacific in the 2CO2 and 4CO2 experiments.

The greenhouse warming is associated with a poleward expansion of the tropical warm SSTs. In particular, the 26 ^{o}C isotherm, that we know to be crucial for the development of the TCs, in the 4CO2 case migrates polward of almost 10^{o} latitude compared to the PREIND one. In the model, however, the warming of the subtropical and mid-latitudes is not accompanied by a poleward extension of the TC action. The peaks of TC activity remain substantially confinedequatorward of 20^{o} latitude in both the Hemispheres.

Despite the reduced number of TCs generated when the CO2 has doubled and quadrupled, there are evidences of an increase in their intensity, at least in terms of precipitation.

Bibliography

Anthes R.A., Corell R.W., Holland G., Hurrel J.W., MacCracken M.C., and K.E. Trenberth, 2006: Hurricanes and Global Warming - Potential Linkages and Consequences. Bul l. Am. Meteor. Soc., DOI:10.1175/BAMS–87–5–617

Aiyyer, A.R., and C. Thorncroft 2006: Climatology of vertical wind shear over the tropical Atlantic J. of Clim., 19, 2969–2983

Behera S.K., J.J. Luo JJ, S. Masson, P. Delecluse, S. Gualdi, A. Navarra, T. Yamagata, 200: Paramount impact of the Indian Ocean dipole on the East African short rains: A CGCM study. J. of Clim., 18, 4514–4530

Bengtsson L., M. Botzet, M. Esch, 1995: Hurricane–type vortices in a general–circulation model. Tel lus-A 47, 175–196

Bengtsson L., M. Botzet, M. Esch, 1996: Will greenhouse gas–induced warming over the next 50 years lead to higher frequency and greater intensity of hurricanes? Tel lus-A, 48, 57–73

Blanke B., P. Delecluse, 1993: Low frequency variability of the tropical Atlantic ocean simulated by a general circulation model with mixed layer physics. J. Phys. Oceanogr., 23, 1363–1388

Broccoli A.J., and S. Manabe, 1990: Can existing climate models be used to study anthropogenic changes in tropical cyclone climate. Geophys. Res. Lett., 17, 1917–1920

Camargo S.J., A.G. Barnston, and S.E. Zebiak, 2004: Properties of Tropical Cyclones in atmospheric general circulation models. IRI Tech. Rep. 04-02, International Research Institute for Climate Prediction, Palisades, N.Y. 72 pp

Chan J.C.-L., 2000: Tropical cyclone activity over the western North Pacific associated with El Nino and La Ni ˜na events. J. of Clim., 13, 2960–2972

Chauvin F., J.-F. Royer, and M. Deque, 2006: Response of hurricane-type vortices to global warming as simulated by ARPEGE-Climat at high resolution. Clim. Dyn., 27, 377–399

Chia H.H, and C.F. Ropelewski, 2002: The interannual variability in the genesis location of tropical cyclones in the northwest Pacific. J. of Clim., 15, 2934–2944

De Maria, M, J.A. Knaff, and B.H. Connell, 2001: A Tropical Cyclone Genesis Parameter for the Tropical Atlantic. Weath. Forec., 16, 219–233

Dutton, J. F., C. J. Poulsen, J. L Evans, 2000: The effect of global climate change on the region of tropical convection in CSM1. Gophys. Res. Lett., 27, 3049–3052

Elsner J.B., and B. Kocher, 2000: Global tropical cyclone activity: A link to the North Atlantic Oscillation. Gophys. Res. Lett., 27, 129–132

Emanuel K., 1987: The dependence of hurricane intensity on climate. Nature, 326, 483–485

Emanuel K., 2003: Tropical Cyclones. Annu. Rev. Earth Planet. Sci., 31, 75–104

Emanuel K., 2005: Increasing destructiveness of tropical Cyclones over the past 30 years. Nature, bf 436, 686–688

Fichefet T, M. A. Morales-Maqueda, 1999: Modelling the influence of snow accumulation and snow–ice formation on the seasonal cycle of the Antarctic sea-ice cover. Clim. Dyn., 15, 251–268

Gent P.R., and J.C. McWilliams, 1990: Isopycnal mixing in ocean circulation models. J. Phys. Ocean., 20, 150–155

Goldenberg S.B., C.W. Landsea, A.M. Mestas-Nu˜nez, and W.M Gray, 2001: The recent increase in the Atlantic hurricane activity: causes and implications. Science, 293, 474–479

Goldenberg S.B., L.J. Shapiro, 1996: Physical mechanisms for the association of El Nino and west African rainfall with Atlantic ma jor hurricane activity. J. of Clim, 9, 1169–1187

Gray W.M., 1968: Global view of the origin of tropical disturbances and storms. Mon. Wea. Rev., 96, 669-700

Gray W.M., 1979: Hurricanes: Their formation, structure and likely role in the tropical circulation. Meteorology over the Tropical Oceans, D.B. Shaw (Ed.), Royal Meteorological Society, 155–218

Gray W.M., 1984: Atlantic seasonal hurricane frequency .1. El-Nino and 30-mb Quasi–biennial oscillation influences. Mon. Weather Rev., 112, 1649–1668

Gualdi, S., A. Navarra, E. Guilyardi, and P. Delecluse, 2003a: Assessment of the tropical Indo-Pacific climate in the SINTEX CGCM, Ann. Geophysics, 46, 1–26

Gualdi, S., E. Guilyardi, A. Navarra, S. Masina, and P. Delecluse, 2003b: The interannual variability in the tropical Indian Ocean as simulated by a CGCM. Clim. Dyn., 20, 567–582

Guilyardi, E., P. Delecluse, S. Gualdi, and A. Navarra, 2003: Mechanisms for ENSO phase change in a coupled GCM, J. of Clim., 16, 1141–1158

Haarsma R.J., J.F.B. Mitchell, C.A. Senior, 1993: Tropical disturbances in a GCM. Clim. Dyn., 8, 247–257

Holland G.J., 1993: ”Ready Reckoner” - Chapter 9, Global Guide to Tropical Cyclone Forecasting, WMO/TC-No. 560, Report No. TCP-31, World Meteorological Organization; Geneva, Switzerland

Holland G.J., 1997: The maximum potential intensity of tropical cyclones. J. Atmos. Sci.,

54, 2519–2541

Jones, P.D., D.E. Parker, T.J. Osborn, and K.R. Briffa. 2006: Global and hemispheric temperature anomalies–land and marine instrumental records. In Trends: A Compendium of Data on Global Change. Carbon Dioxide Information Analysis Center, Oak Ridge National Laboratory, U.S. Department of Energy, Oak Ridge, Tenn., U.S.A.

Knutson T.R., and R.E. Tuleya, 2005: Reply. J. of Clim., 18, 5183–5187

Knutson T.R., and R.E. Tuleya, 2004: Impact of CO2 induced warming on simulated hurricane intensity and precipitation: sensitivity to the choice of climate model and convective parametrization. J. of Clim., 17, 3477–3495

Knutson T.R., R.E. Tuleya, W. Shen, and I. Ginis, 2001: Impact of CO2–induced warming on hurricane intensities simulated in a hurricane model with ocean coupling. J. of Clim., 14, 2458–2468
Landsea C.W., B.A. Harper, K. Hoarau, and J. Knaff, 2006: Can we detect trends in extreme tropical cyclones?, Science, 313, 452–454

Latif M., N. Keenlyside, J. Bader, 2007: Tropical sea surface temperature, vertical wind shear, and hurricane development. Geophys. Res. Lett., 34, L01710

Luo, J.-J., S. Masson, S. Behera, P. Delecluse, S. Gualdi, A. Navarra, and T. Yamagata, 2003: South Pacific origin of the decadal ENSO-like variation as simulated by a coupled GCM.

Geop[hys. Res. Lett., 30, 2250, doi:10.1029/2003GL018649
Madec, G., P. Delecluse, M. Imbard, and C. Levy, 1999: OPA 8.1 Ocean General Circulation Model reference manual, Internal Rep. 11, Inst. Pierre–Simon Laplace, Paris, France

Masson S., Impact of barrier layer on winter–spring variability of the southeastern Arabian Sea. Geophys. Res. Lett., 32, L07703, doi:10.1029/2004GL021980

Michaels P.J., P.C. Knappenberger, and C Landsea, 2005: Comments on ”impacts of CO2–induced warming on simulated hurricane intensity and precipitation: Sensitivity to the choice of climate model and convective scheme”. J. of Clim., 18, 5179–5182

Mocrette J.J., 1991: Radiation and cloud radiative properties in the European centre for medium range weather forecasts forecasting system. J. Geophys. Res., 96, 9121–9132

Nordeng T.E., 1994: Extended versions of the convective parametrization scheme at ECMWF and their impact on the mean and transient activity of the model in the Tropics. ECMWF Research Department, Technical Memorandum No. 206, October 1994, European Center for Medium Range Weather Forecasts, Reading, UK, 41 pp

Palmen, E., 1948: On the formation and structure of tropical hurricanes. Geophysica, 3, 26-39

Pielke Jr. R., C. Landsea, M. Mayfield, J. Laver, and R. Pasch, 2006: Reply to "Hurricanes and Global Warming - Potential Linkages and Consequences. Bul l. Am. Meteor. Soc., DOI:10.1175/BAMS-87-5-622

Pielke Jr. R., C. Landsea, M. Mayfield, J. Laver, and R. Pasch, 2005: Hurricanes and Global Warming. Bul l. Am. Meteor. Soc., DOI:10.1175/BAMS-86-11-1571

Rayner N.A., D.E. Parker, E.B. Horton, C.K. Folland, L.V. Alexander, D.P. Rowell, E.C. Kent, and A. Kaplan, 2003: Global analyses of sea surface temperature, sea ice, and night marine air temperature since the late nineteenth century. J. Geophys. Res., 108, D14, 4407, doi:10.1029/2002JD002670

Roeckner E, and Coauthors (1996) The atmospheric general circulation model Echam-4: model description and simulation of present-day climate. Max-Planck-Institut f fur Meteorologie, Rep. No 218, Hamburg, Germany, 90 pp

Roullet G., and G. Madec, 2000: Salt conservation, free surface, and varying levels: a new formulation for ocean general circulation models. J. Geophys. Res, 105, 23927–23942

Royer J.-F., F. Chauvin, B. Timbal, P Araspin, and D. Grimal, 1998: A GCM study of the impact of greenhouse gas increase on the frequency of occurrence of tropical cyclones. Clim Dyn., 38, 307–343

Sugi M., A. Noda, N. Sato, 2002: Influence of global warming on tropical cyclone climatology: an experiment with the JMA global model. J. Meteor. Soc. Japan, 80, 249–272

Sugi M., and J. Yoshimura, 2004: A mechanism of tropical precipitation change due to C O_2 increase. J. of Clim, 17, 238–243

Tiedtke M., 1989: A comprehensive mass flux scheme for cumulus parametrization in large– scale models. Mon. Weather Rev., 117, 1779–1800

Timmermann R., H. Goosse, G. Madec, T. Fichefet, C Ethe and V. Dulie're, On the representation of high latitude processes in the ORCALIM global coupled sea ice-ocean model, Ocean Modell., 8, 175-201, 2005

Trenberth K., 2005: Uncertainty in Hurricanes and Global Warming. Science, 308, 1753–1754

Vecchi G.A., B.J. Soden, 2007: Global Warming and the Weakening of the Tropical Circulation. J. of Clim., submitted.

Walsh K.J.E, 1997: Objective detection of tropical cyclones in high–resolution analyses. Mon. Weather Rev., 120, 958–977

Walsh K.J.E., and B.F. Ryan, 2000: Troipcal cyclone intensity increase near Australia as a result of climate change. J. of Clim., 13, 3029–3036

Walsh K.J.E., 2004: Tropical cyclones and climate change: unresolved issues. Clim. Res.,

22, 77–83

Webster P.J., G.J. Holland, J.A. Curry, and H.-R. Chang, 2005: Changes in Tropical Cyclones Number, Duration and Intensity in a Warming Environment. Science, 309, 1844–1846.

Xie P., and P. Arkin, 1997: Global precipitation: A 17-year monthly analysis based on gauge observations, satellite estimates, and numerical model outputs. Bul l. Am. Meteor. Soc., 78, 2539–2558

Yoshimura J., M. Sigu, and A. Noda, 2006: Influence of greenhouse warming on tropical cyclone frequency. J. Meteor. Soc. Japan, 84, 405–428

Tables and Figures

CLIMATE SIMULATIONS AND SCENARIOS		
Name	**Experiment**	**Length of the analyzed time series**
PREIND	Preindustrial ghg concentration	30 years
20C3M	20th Century ghg conc + aerosols	30 years (1970-1999)
2CO2	2 x PREIND CO_2 conc.	30 years
4CO2	4 x PREIND CO_2 conc.	30 years

Table 1: Summary of the climate simulations used in this study.

NUMBER OF TCs 1970-1999		
	OBS	**SXG 20C3M**
TOT	2813	1986
MEAN	93.8	66.2
STD	10.9	9.2

Table 2: Total number of Tropical Cyclones found in the observations and in the 20th Century model simulation during the period 1970-1999.

	PREIND	2CO2	4CO2
$T_{global\ mean}$ [^oK]	288.37	299.377 (+2.01%)	292.72 (+4.36)
$T_{Tropics}$ [^oK]	298.72	300.286 (+1.57%)	302.41 (+3.69)
$Prec_{global\ mean}$ [mm/day]	2.757	2.809 (+1.89%)	2.852 (+3.45%)
$Prec_{Tropics}$ [mm/day]	3.317	3.353(+1.09%)	3.354 (+1.12%)
$ConvPrec_{global\ mean}$ [mm/day]	1.209	1.164 (-3.72%)	1.106 (-8.52%)
$ConvPrec_{Tropics}$ [mm/day]	2.117	2.008 (-5.15%)	1.884 (-11.01%)

Table 3: Global average and tropical average of mean surface temperature, mean total precipitation and mean convective precipitation. The mean have been computed over the 30-year periods considered in the study. Values in parenthesis are the differences (absolute values for temperature and percentage for precipitation) with respect to the PREIND case.

	Number of Tropical Cyclones			Number of Tropical Cyclone Days		
	PREIND	2CO2	4CO2	PREIND	2CO2	4CO2
TOT	2196.0	1839.0	1229.0	51941.0	5085.0	3313.0
MEAN	73.2	61.3	41.0	98.0	169.5	110.4
STD	6.8	8.3	7.6	22.5	24.0	23.3

Table 4: Total number of TCs (left columns) and total number of TC days (right columns) found in the PREIND, 2CO2 and 4CO2 experiments. In all of the experiments a 30-year period is considered. In the upper row is the total number of TCs and TC days; in the middle row is the mean number of TCs and TC days per year; in the bottom row is the year-to-year standard deviation of the annual number of TCs and TC days.

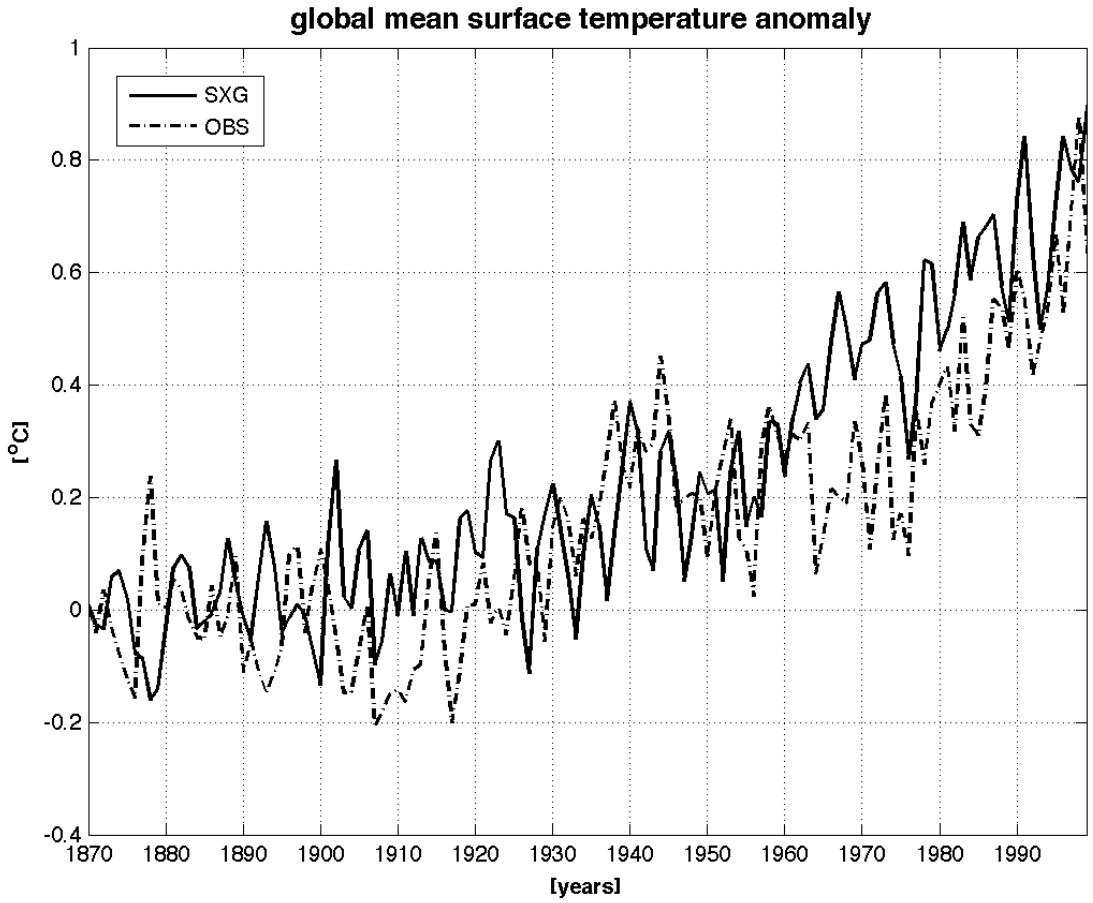

Figure 1: Time series of the annual mean values of surface temperature averaged over the entire globe. The values plotted are the year-to-year deviation with respect to the 1870-1890 mean. Dashed line are the observations; solid line the model simulation.

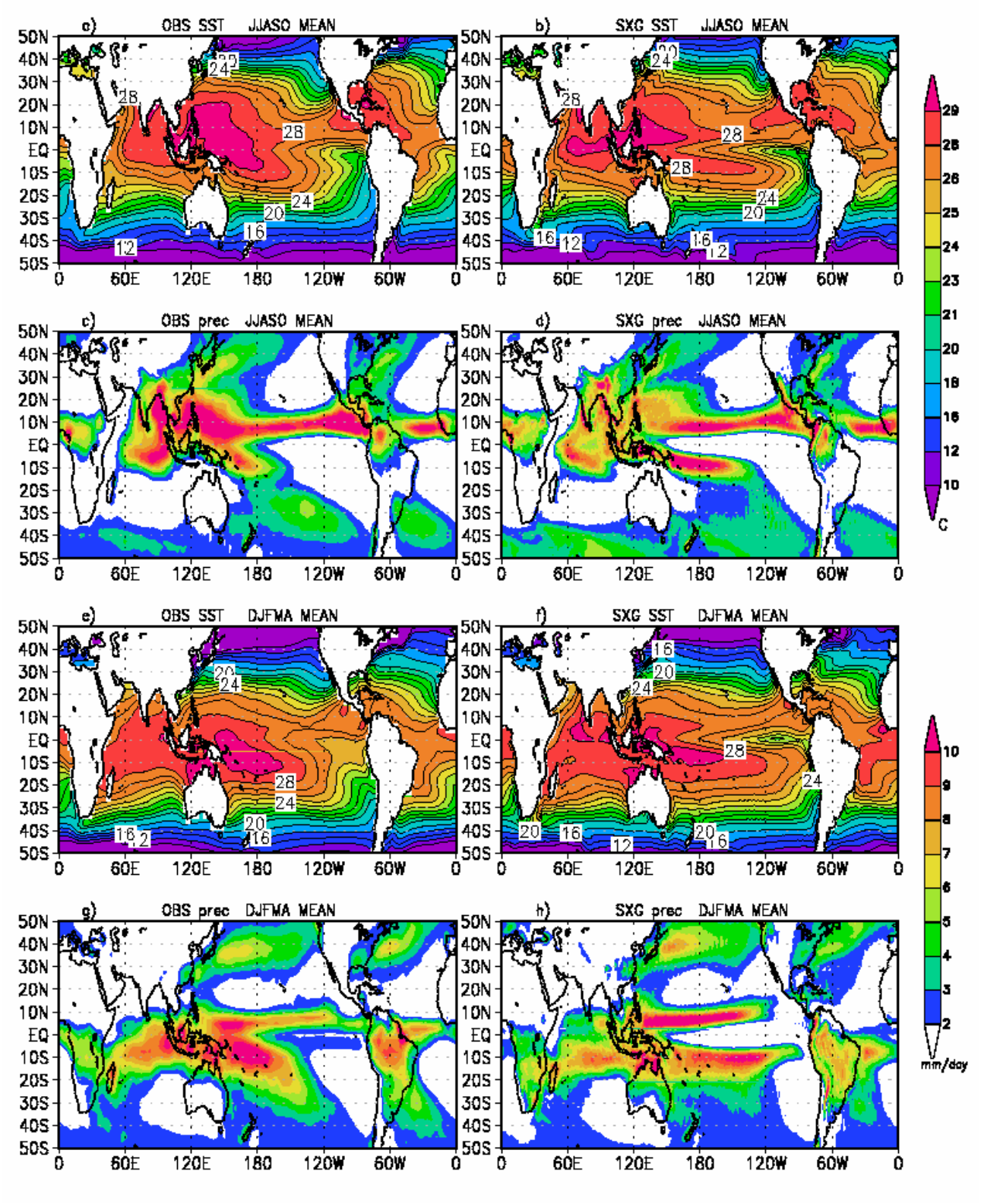

Figure 2: Seasonal means of sea-surface temperature (SST) and precipitation as obtained from the observations (left panels) and the model (right panels). The upper panels (a-d) show the extended Northern Hemisphere summer means June-July-August-September-October (JJASO); the lower panels (e-h) are the means obtained for the extended Southern Hemisphere summer December-January-February-March-April (DJFMA). The

SST contours (panels a, b, e and f) are 2 °C. The precipitation contours (panels c, d, g and h) are 1 mm/day. Rainfall values lower than 2 mm/day are not plotted.

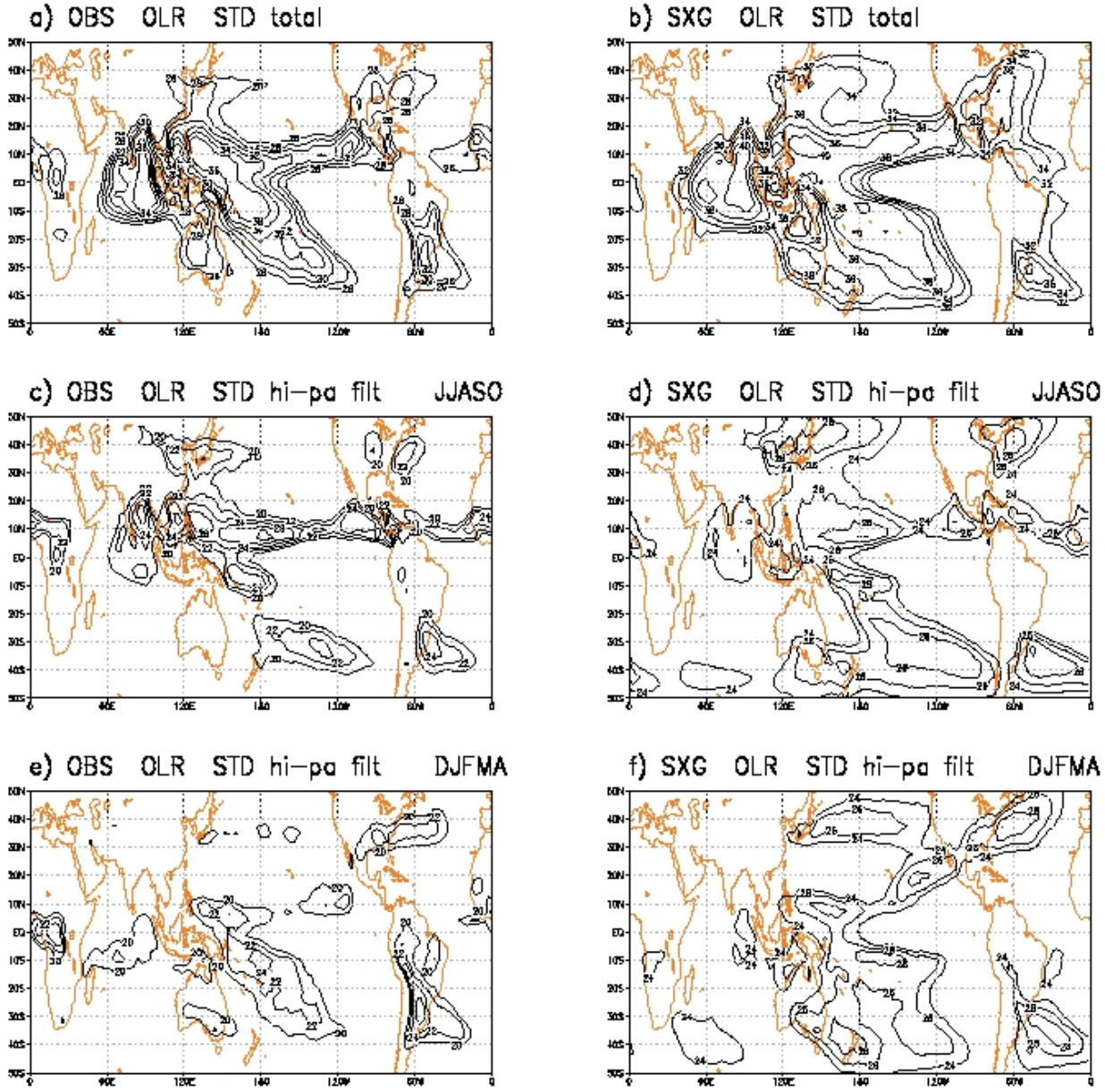

Figure 3: Standard deviation of the outgoing longwave radiation (OLR) obtained from daily anomalies for the period 1979-2000 for the observations (left panels) and 1970-2000 for the model (right panels). Upper panels (a and b) show the standard deviation of the total anomalies. Middle panels (c and d) show the standard deviation of the high-pass filtered anomalies for the northern summer (JJASO). Bottom panels show the results from the high-pass filtered anomalies for the southern summer (DJFMA). The filtered anomalies have been obtained by applying a Fourier filter to suppress signals with periods longer than 25 days. The contour lime interval is 2 W/m2

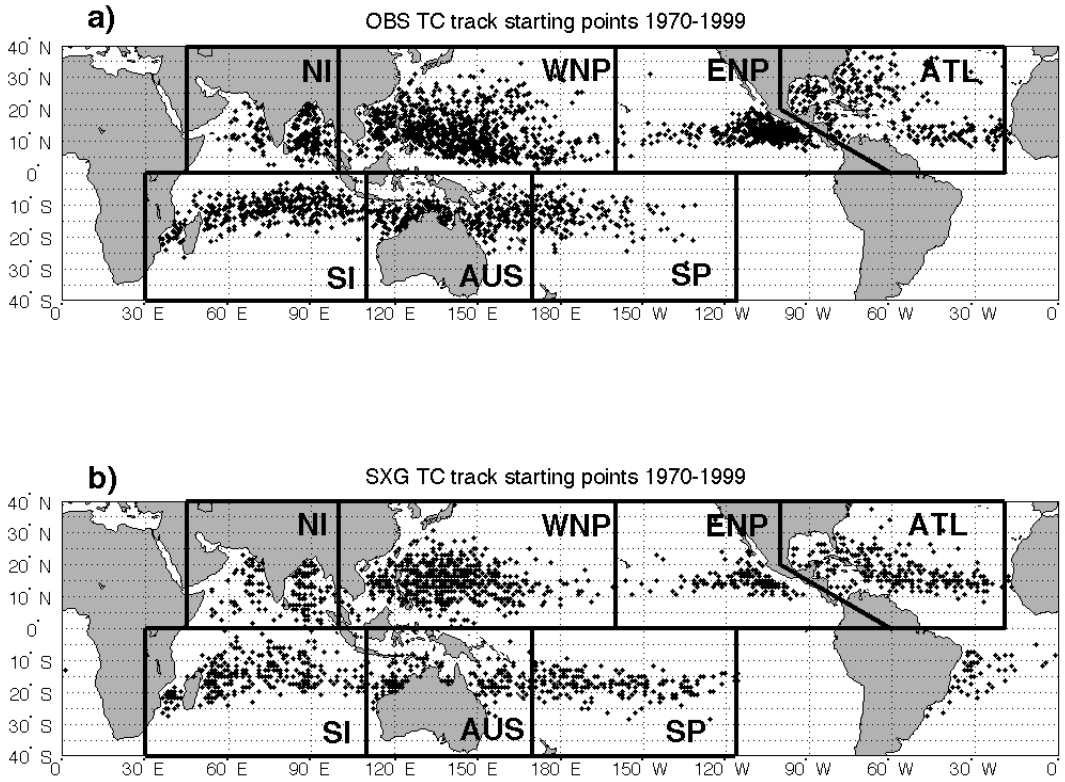

Figure 4: Distribution of the TC track starting points for the period 1970-1999 for the observations (panel a) and model (panel b). Each point corresponds to the geographical location of a TC at the time of its first detection. Following Camargo et al. (2004) seven regions of TC genesis have been defined. In the pictures these regions are delimited by thick black lines.

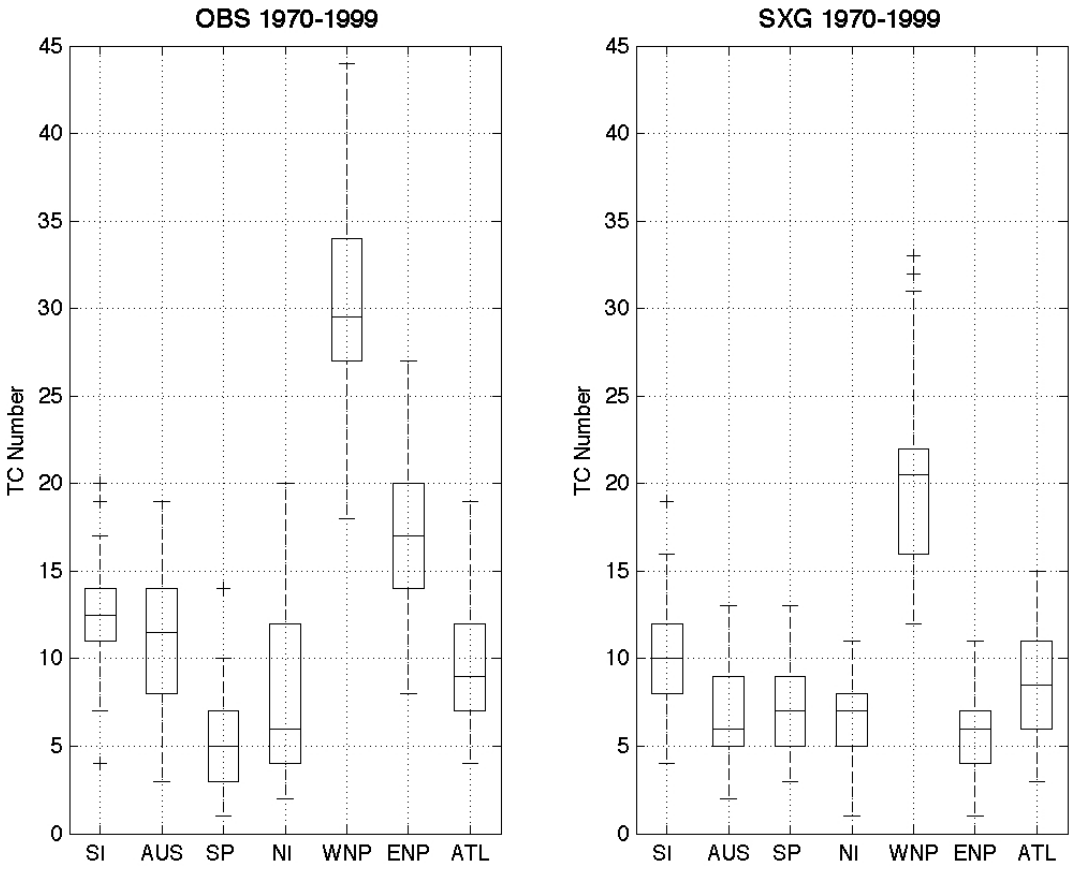

Figure 5: Box plots of the number of TCs per year for the observations (left panel) and model simulation (right panel). The number of TCs (y-axis) is plotted for each area of TC-genesis (x-axis) defined in Figure 4.

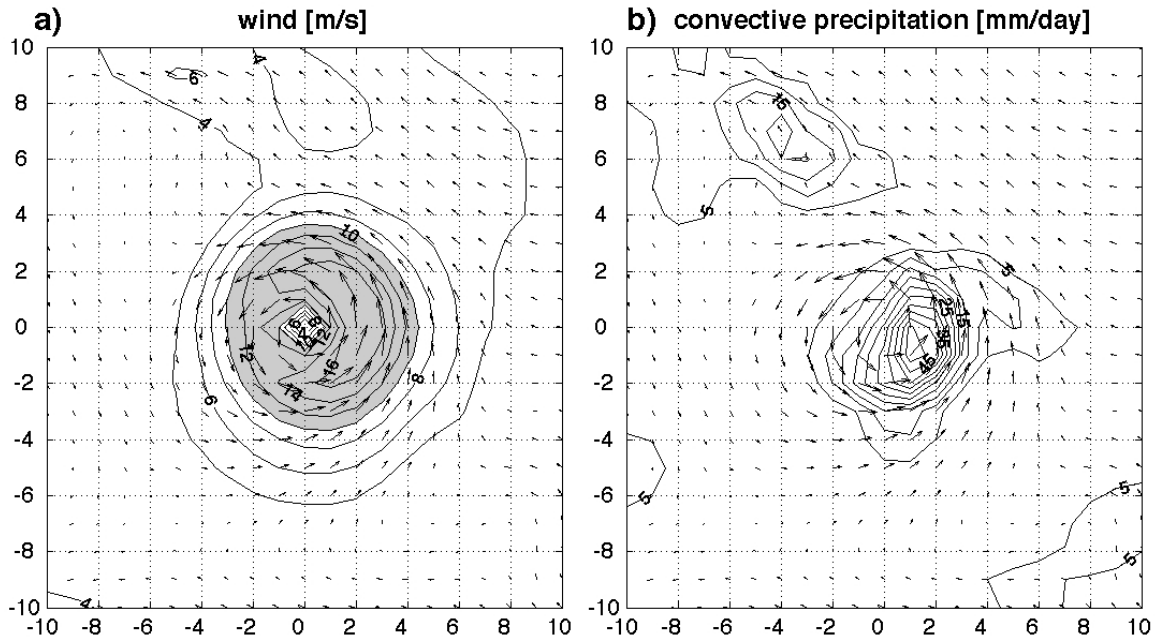

Figure 6: Composite patterns of 850-hPa wind and convective precipitation associated with a simulated TC. The composite have been computed by averaging the fields over the period of occurrence of the TC and for a spatial domain centred in the core of the cyclone and extending 10° each side. In panel a) the of 850-hPa wind (arrows) is plotted along with the intensity of the wind (contour). The contour interval is 2 m/s. Contours larger than 10 m/s are shaded. Panel b) shows the 850-hPa wind (arrows) along with the convective precipitation rate. The contour interval is 5 mm/day.

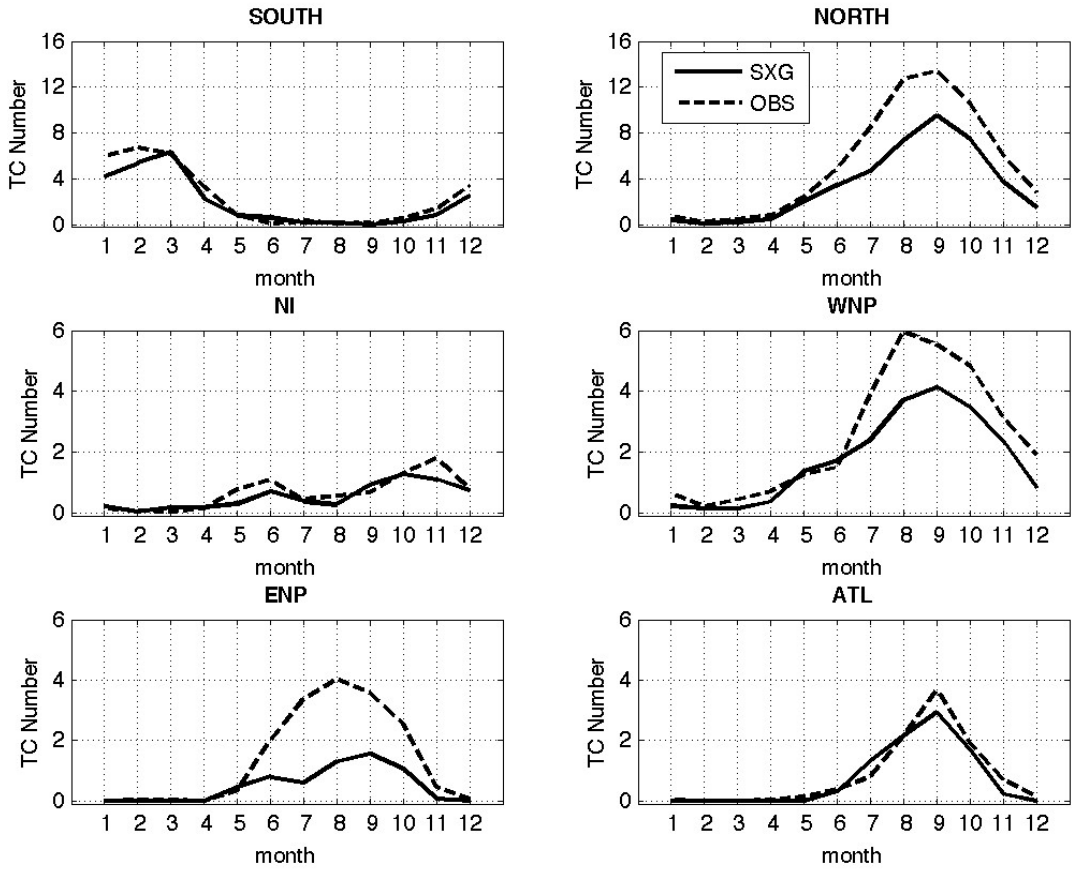

Figure 7: Seasonal modulation of the TC occurrence for the observations (dashed lines) and model simulation (solid lines) and for different region of the Tropics. Upper panels: tropical region of the Southern Hemisphere (left) and of the Northern Hemisphere (right). Middle and lower panels: northern Indian Ocean, western tropical Pacific, eastern tropical Pacific and tropical Atlantic.

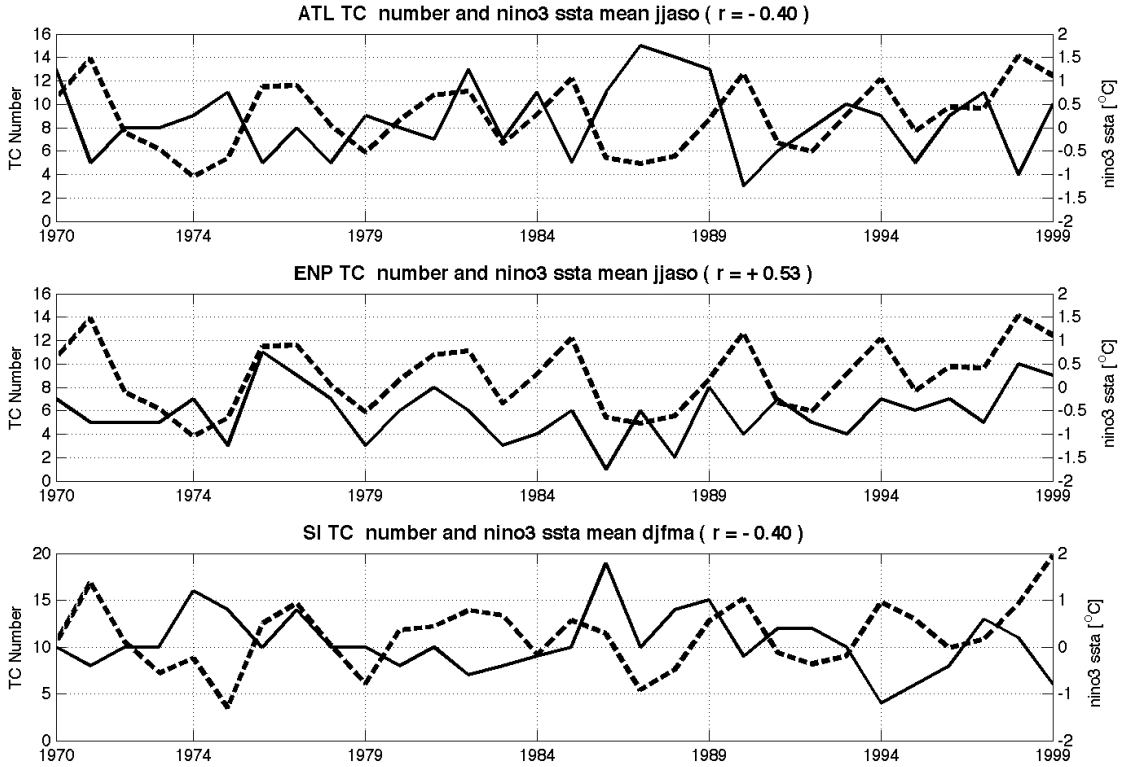

Figure 8: Time series of the number of TCs along with the NINO-3 index for different regions of the Tropics. The dashed lines show the interannual variation of the number of simulated TCs in the northern tropical Atlantic (upper panel), northern tropical eastern Pacific (middle) and Southern Indian Ocean (lower panel). The solid line show the value of NINO-3 SSTA index defined as the average of the SST anomaly over the NINO-3 region (5°S-5°N ; 150°W-90°W). The values of the NINO-3 index plotted in the ATL and ENP case have been obtained for JJASO, whereas for the SI case it has been computed for DJFMA. The value of the correlation between the two curves (r) is also shown.

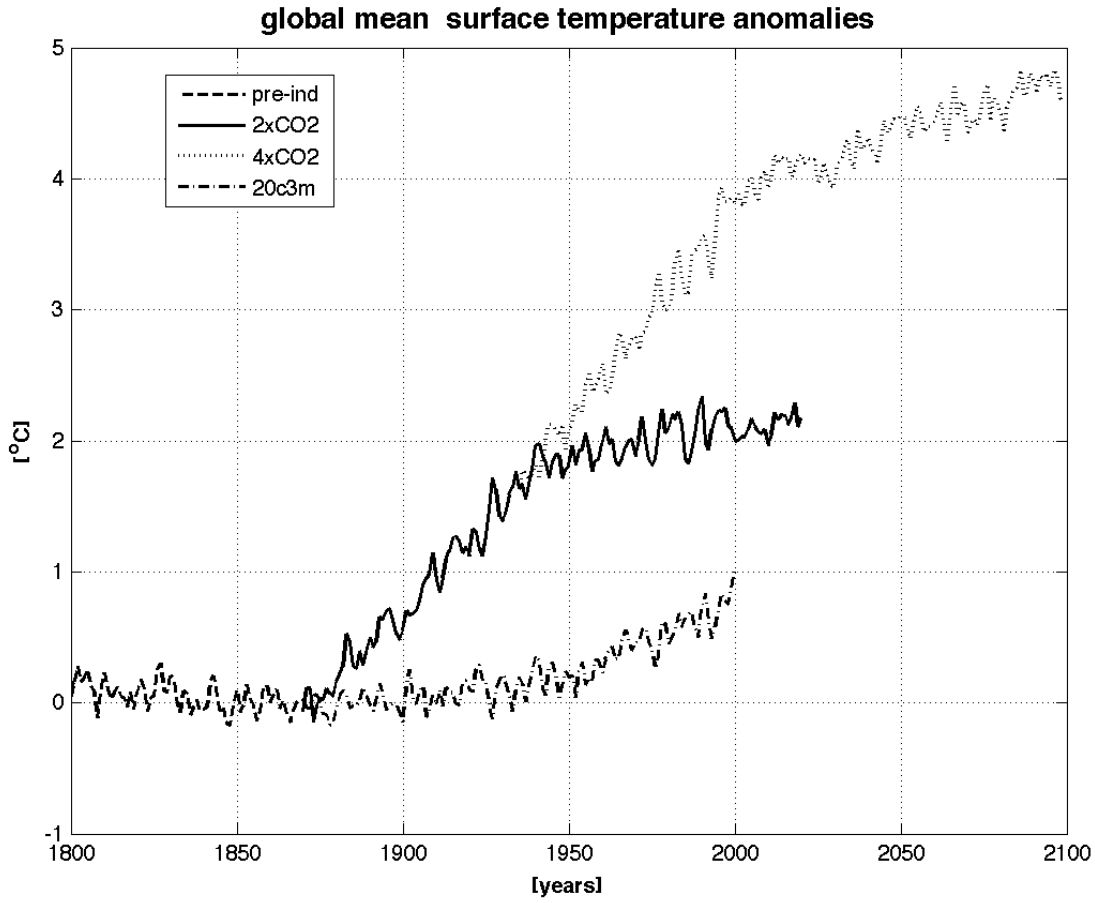

Figure 9: Time series of the annual mean values of surface temperature averaged over the entire globe for the pre-industrial (PREIND) simulation (dashed curve), the 20th Century simulation (20C3M, dashed and dotted curve), the 2CO2 experiment (solid line) and the 4CO2 experiment (dotted curve). The values plotted are the year-to-year deviation with respect to the 1870-1890 mean.

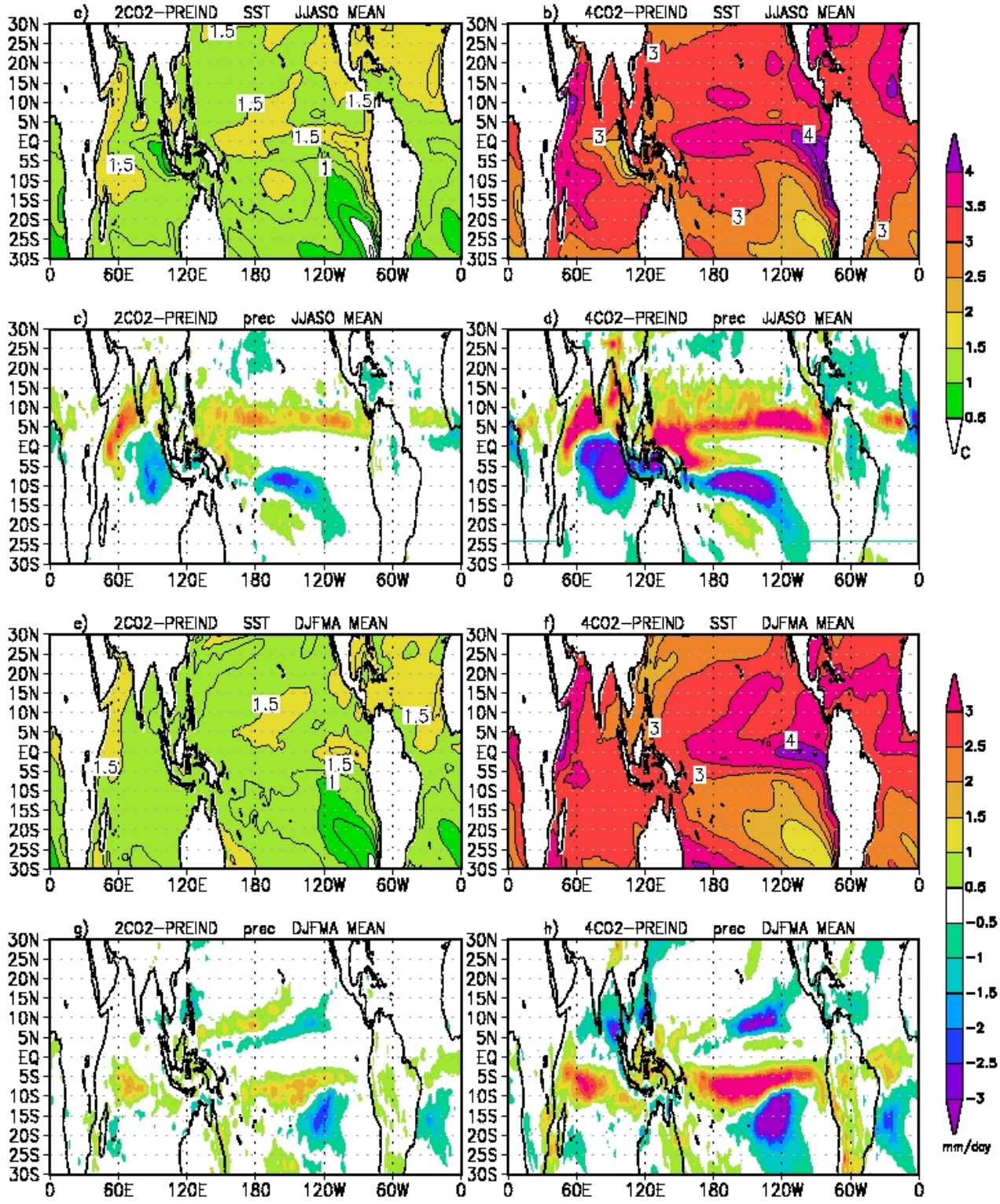

Figure 10: Differences between the seasonal mean SST and precipitation obtained from the 2CO2 and PREIND experiments (left panels) and 4CO2 and PREIND experiments (right panels). Panels a, b, e and f show the differences in mean SST; contour interval is 0.5 °C. Panels c, d, g and h show the differences in mean precipitation, with a contour interval of 0.5 mm/day.

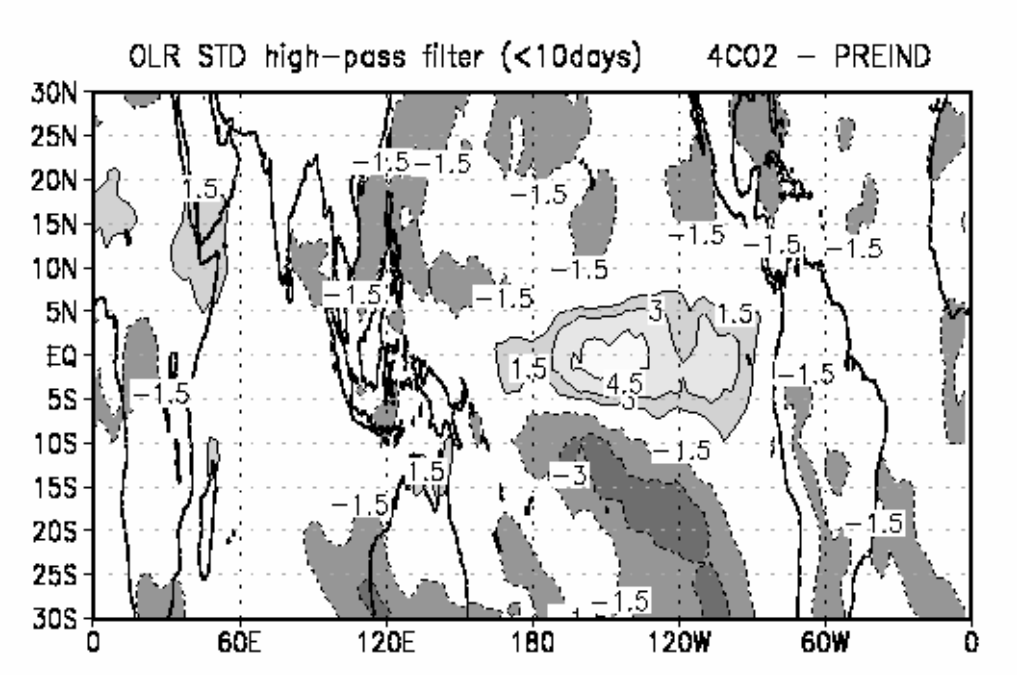

Figure 11: Difference between the standard deviation of the high-pass filtered outgoing longwave radiation (OLR) anomalies obtained from the 4CO2 and the PRIND experiments. The OLR anomalies have been filtered as explained for Figure 3. Contour interval is 1.5 W/m2. Dashed lines and dark shading indicate negative values of the difference. Solid line and light shading indicate positive values of the difference.

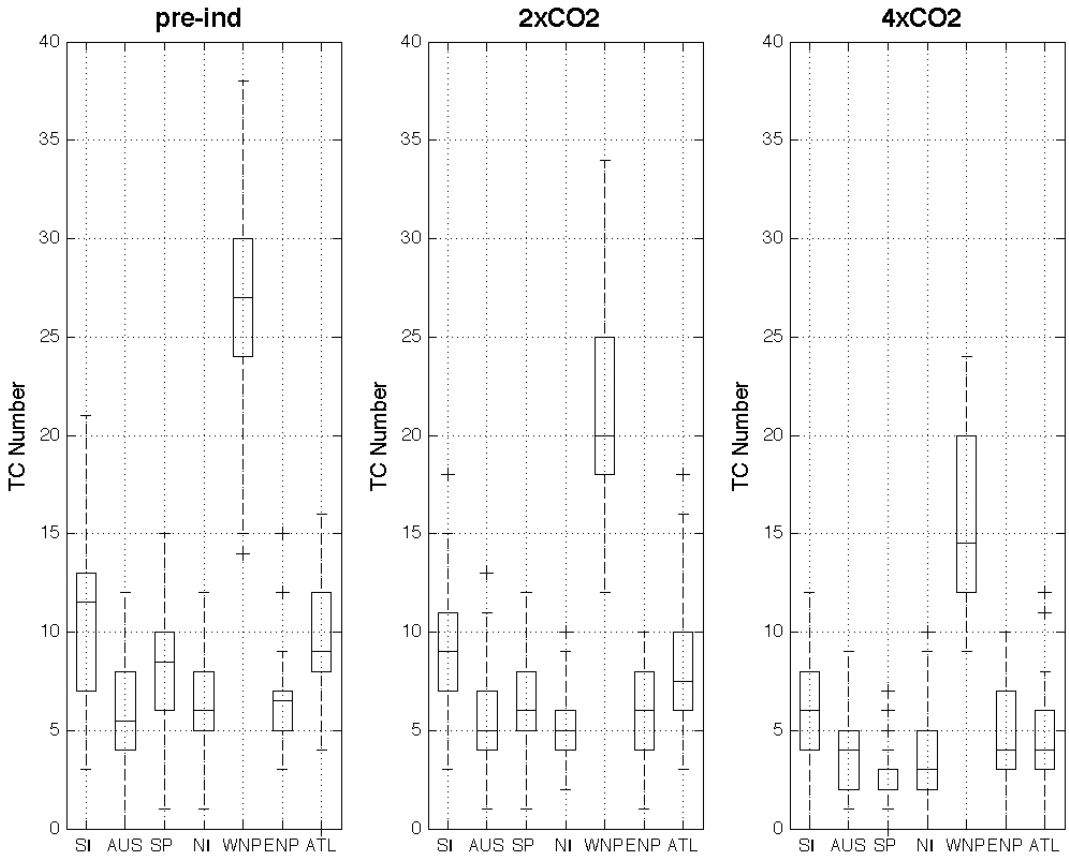

Figure 12: Box plot of the annual number of TCs in the areas defined in Figure 4 and for the PREIND experiment (left panel), 2CO2 experiment (middle) and 4CO2 experiment (right panel).

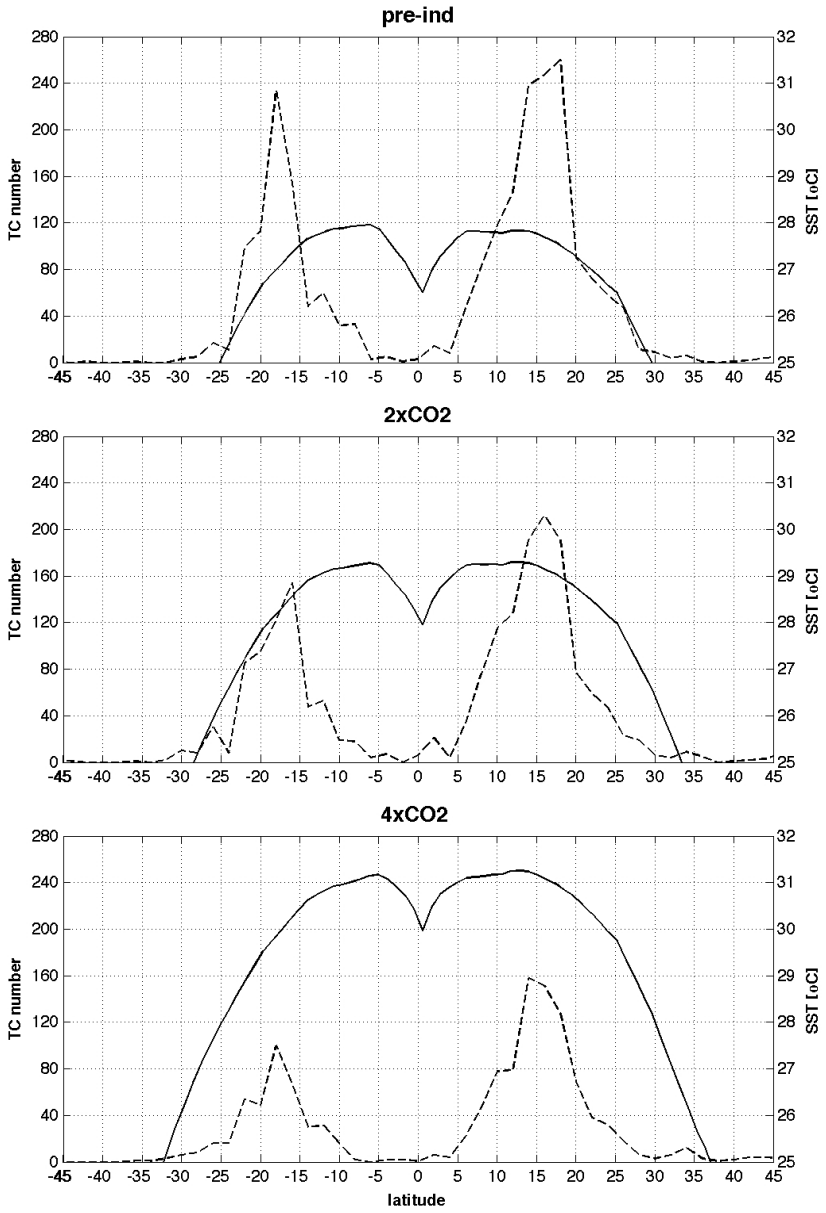

Figure 13: Latitudinal distribution of the total number of simulated TCs and zonal mean value of SST for the PREIND experiment (upper panel), the 2CO2 case (middle panel) and the 4CO2 experiment (lower panel). On the x-axis is the latitude. The y-axis on the left show the number of TCs and on the right the SST value. The dashed curve shows the meridional distribution of the total number of TCs, with two maxima centred between 15°and 20° latitude in both the Hemispheres. The solid curve shows the distribution of the zonal mean SST. The two curves indicate, for each latitude, the number of TCs and the value of the SST.

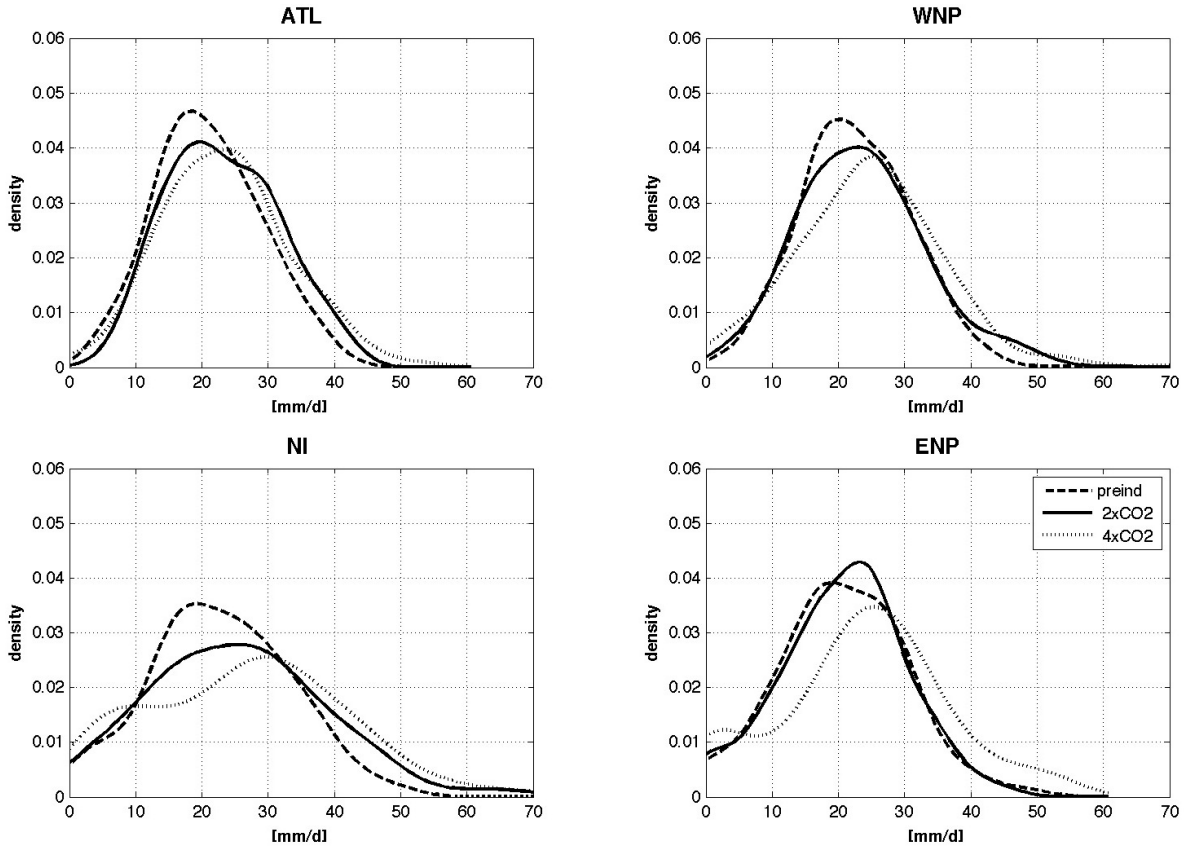

Figure 14: Probability distribution function (PDF) of convective precipitation associated with the simulated TCs in the different regions for the PREIND case (dashed line), 2CO2 case (solid line) and 4CO2 experiment (dotted line). On the x-axis is the value of convective precipitation in mm/day. On the y-axis is the (density of) frequency of events corresponding to a certain amount of convective rainfall.

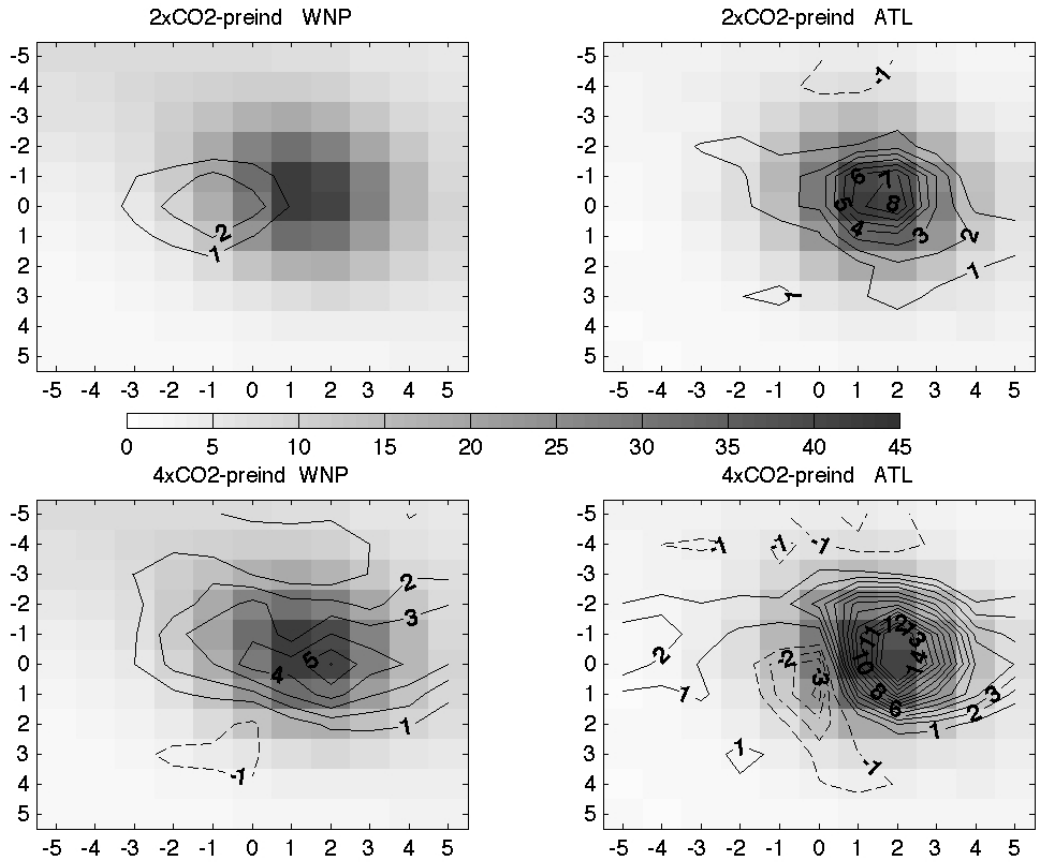

Figure 15: Left panels: composite of TC precipitation for the PREIND experiment over the WNP region (shaded pattern) along with the difference 2CO2-PREIND (upper panel) and 4CO2-PREIND (lower panel) shown by the contour patterns. Right panels: as for the left panels but for the ATL region. The PREIND rainfall composite (shaded patterns) have a shaded contour interval of 5 mm/day. The difference between the 2CO2 and PREIND composite and the 4CO2 and PREIND composite (contour patterns) have a contour interval of 1 mm/day. A test based on the boot-strap technique shows that the difference values plotted in the picture are significant at the 5% level.

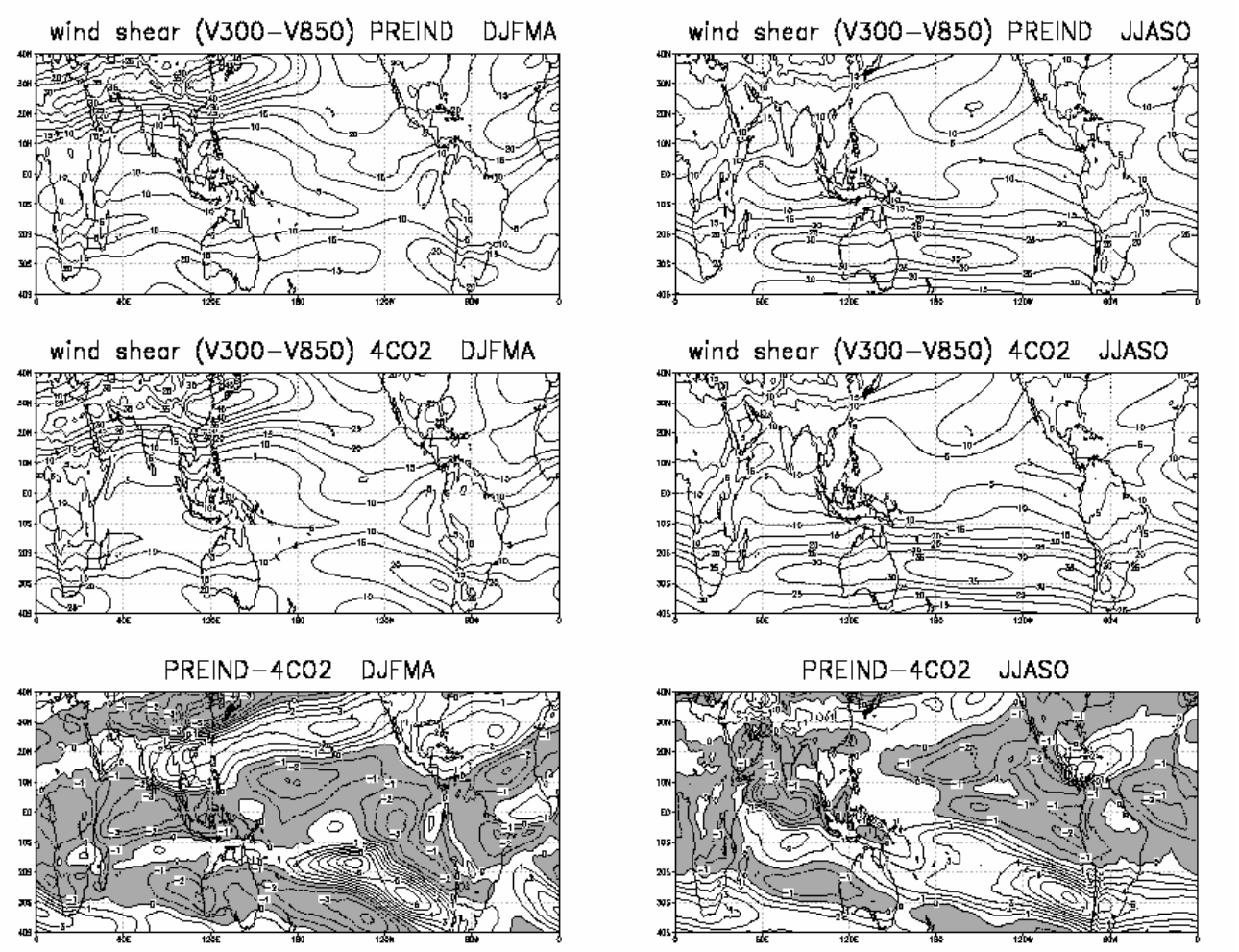

Figure 16: Seasonal mean of the vertical wind shear defined as the difference between the wind at 300 hPa and at 850 hPa. On the left panels are the results for the Southern Hemisphere extended summer (DJFMA), whereas on the right panels the values for the Northern Hemisphere extended summer (JJASO). The upper panels show the fields for the PREIND experiment. The middle panels the results from the 4CO2 experiments. For these plots, the contour interval is 5 m/s. The lower panels show the difference between the 4CO2 and the PREIND case. For these plots the contour interval is 1 m/s and negative values are shaded.

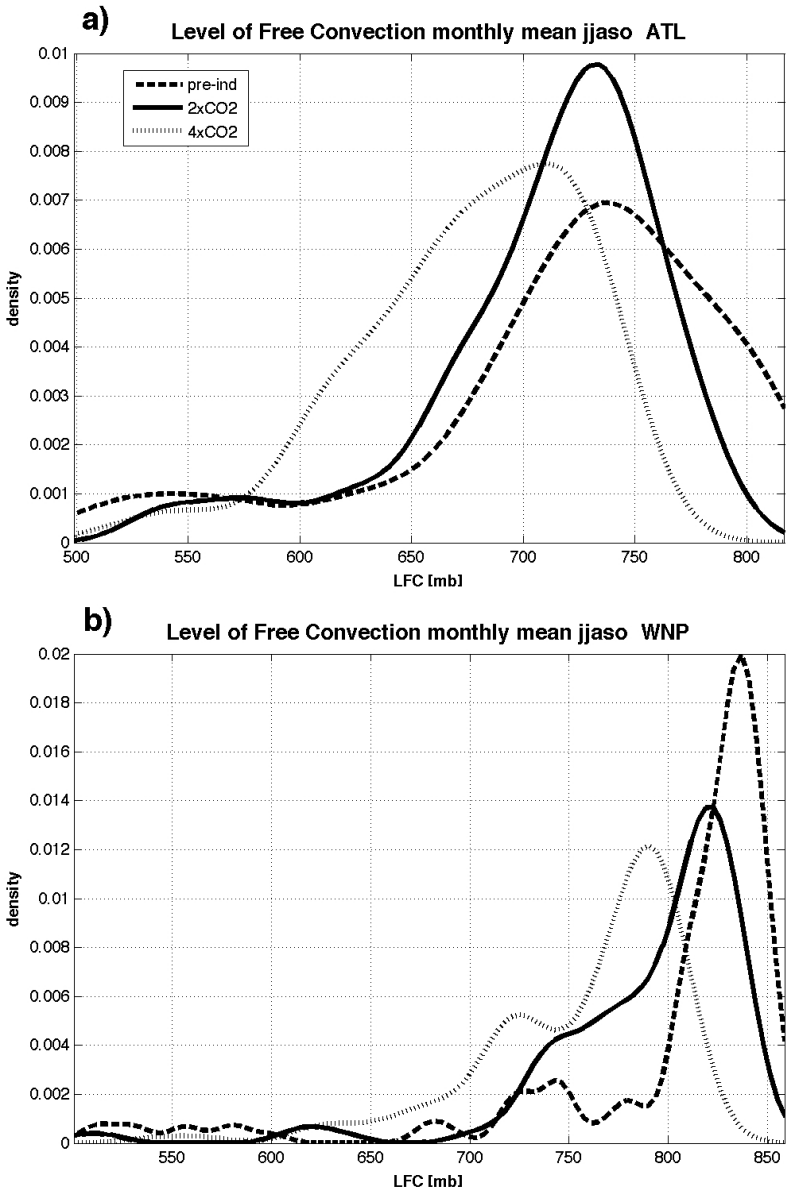

Figure 17: Probability distribution function (PDF) of the level of free convection (LFC) for the PREIND case (dashed), the 2CO2 case (solid line) and the 4CO2 experiment (dotted curve) over the ATL region (panel a) and the WNP region (panel b) during northern summer (JJASO). On the x-axis is the value of vertical levels in Millibar (mb), and on the y-axis is the (density of) frequency of occurrence at which free convection can be triggered at that level.